POLITECNICO DI TORINO

FACOLTA' DI INGEGNERIA

Tesi di laurea magistrale in Ingegneria Energetica e Nucleare

OPTIMIZATION OF PERSONAL DOSIMETRY OF MEDICAL STAFF WEARING RADIOPROTECTIVE GARMENTS

RELATORI

Prof. Gianni Coppa

MSc. Clarita Saldarriaga Vargas

CANDIDATA

Corinne Amalberto

SCK•CEN
STUDIECENTRUM VOOR KERNENERGIE
CENTRE D'ÉTUDE DE L'ÉNERGIE NUCLÉAIRE

Belgian Nuclear Research
Centre (SCK•CEN)
Boeretang 200,
2400 Mol, Belgium

5 Aprile 2017

TABLE OF CONTENTS

ABSTRACT

Personal dosimetry plays a very important role in the dose monitoring of medical staff working in interventional radiology and cardiology. In order to shield the radiation scattered in the patient during the examination, medical staff have to wear radiation protection garments like lead aprons and thyroid collars. The effective dose received by the physician and the dose absorbed by the personal whole-body dosimeters worn by her/him are altered by the presence of lead.

Some personal dosimetry methodologies (single and double dosimetry) exist for the evaluation of the effective dose when radioprotective garments are worn. Single dosimetry consists in the use of only one dosimeter worn over or under the apron and the effective dose is evaluated through the division or multiplication of the dose by correction factors. Double dosimetry proposes the combination of the dose received by two dosimeters, one worn over and one under the apron and combines the two doses through an algorithm. Both of these methods are characterized by high uncertainties that can lead to strong overestimations and underestimations.

This study focuses on the design of a whole-body personal dosimeter for the estimation of the effective dose when wearing radioprotective garments made of lead. The innovative feature is that only one dosimeter (worn over the lead apron) is needed to provide a good estimate of the effective dose. In particular, this analysis regards the optimization of dosimeter based on radiophotoluminescent (RPL) detectors.

The project consists in the design of a new dosimeter starting from an existent dosimeter used to estimate the effective dose without lead garments. Filters are inserted and adapted to obtain an estimation of the effective dose as close as possible to the reference values of effective dose with lead garments already calculated. The dose of the dosimeter is estimated from the dose of two detectors that represent all the parts of the body exposed to radiation: the first dose is read in a detecting volume surrounded by low Z material filters and represents tissues and organs which are not covered by radioprotective garments, while the second one is read in a detecting volume surrounded by high Z material filters and represents the parts covered by lead garments.

The objective is to determine a configuration that allows to minimize overestimations and underestimations of the effective dose in all the exposure conditions considered: parallel photon beams with energies between 20 and 120 keV and angles of incidence between 0° and 60°. The new design and its optimization are performed through Monte Carlo simulations using the radiation transport code MCNPX.

The first part of this thesis focuses on the design of a simplified dosimeter, in which two detectors with different filtrations are studied separately and then combined in terms of dose. The second and third parts focus on the design of a realistic dosimeter with its real structure, dimensions and characteristics.

SOMMARIO

La dosimetria personale è fondamentale per il monitoraggio della dose ricevuta dal personale medico durante i trattamenti di radiologia e cardiologia interventistica. I componenti dello staff medico devono indossare indumenti radioprotettivi per proteggersi dalla radiazione diffusa proveniente dal paziente, come per esempio il grembiule di piombo o il collare per la protezione della tiroide. La dose ricevuta dal dosimetro al corpo intero in caso di vicinanza con il piombo è alterata, e per questo motivo è necessaria una ottimizzazione.

Studi recenti hanno proposto due metodologie (singola e doppia dosimetria), le quali mediante l'utilizzo di algoritmi, consentono il calcolo della dose effettiva in presenza di indumenti radioprotettivi. La singola dosimetria prevede l'uso di un solo dosimetro, indossato sopra o sotto il grembiule di piombo, il quale fornisce un valore di dose che viene modificato attraverso la divisione o la moltiplicazione per opportuni fattori correttivi; la doppia dosimetria consiste invece nella combinazione di dosi lette da due dosimetri, uno indossato sopra e uno sotto il grembiule di piombo, per mezzo di algoritmi. Entrambe le metodologie sono caratterizzate da incertezze che provocano problemi di sovrastima e sottostima della dose.

La proposta innovativa riguarda l'utilizzo di un solo dosimetro, indossato sopra il grembiule di piombo e, in particolare, il progetto si occupa dell'ottimizzazione di un dosimetro a radiofotoluminescenza (RPL). Il progetto consiste nel disegnare un nuovo dosimetro, partendo da quello esistente, nel quale introdurre nuovi filtri adattandoli per far sì che la stima della dose effettiva sia più vicina possibile ai valori di riferimento calcolati in presenza di indumenti radioprotettivi. La dose combinata viene calcolata considerando due contributi di dose per tenere in considerazione tutte le parti del corpo esposte alle radiazioni: la prima dose si riferisce al volume di rilevamento circondato da filtri creati con materiali a basso Z e rappresenta i tessuti e gli organi che non sono coperti da indumenti radioprotettivi, mentre la seconda è letta nel volume di rilevamento circondato da filtri ad alto Z e rappresenta le parti coperte dagli indumenti di piombo. Il nuovo progetto e la sua ottimizzazione sono effettuati con simulazioni Monte Carlo utilizzando il codice MCNPX, che permette di determinare l'energia depositata nel detector dovuta all'esposizione da fotoni, tenendo in considerazione il trasporto sia di fotoni sia di elettroni. La prima fase dell'analisi consiste nella progettazione di un dosimetro semplificato in cui i due rilevatori, caratterizzati dai diversi filtri, sono studiati separatamente e poi combinati in termini di dose. La seconda fase di progettazione riguarda l'evoluzione dal dosimetro semplificato ad un dosimetro realistico definito in accordo con la sua vera struttura, le dimensioni e le caratteristiche.

L'obiettivo è determinare la configurazione che consenta di minimizzare le sovrastime e le sottostime della dose effettiva in tutte le condizioni di esposizione; per questo motivo i piani trasversale e sagittale devono essere tenuti in considerazione. Poiché si tratta di una analisi iniziale, l'attenzione si concentra principalmente sul piano trasversale, con una sorgente di fotoni incidente con angoli pari a 0°, 45° e 60° rispetto all'asse.

1. INTRODUCTION

1.1 Radiation protection principles and dose limits

Medical staff working in interventional radiology (IR) and cardiology (IC) are exposed to scattered ionizing radiation. There are three main principles on which radiation protection can be assessed: distance, shielding and time. Shielding is the most relevant in this particular analysis and it consists on personal and room protective equipment: glasses, thyroid collar, lead apron, ceiling suspended shield, table shield and mobile shield. All radiation exposures should be kept as low as reasonably achievable (ALARA), taking into account economic and societal factors; ALARA is a function of risk and frequency of the events. ICRP (International Commission on Radiological Protection) has defined limits in terms of dose, for public and workers separately, in a period of one year. The absorbed dose (D) is the fundamental physical quantity and in radiation biology, clinical radiology and radiological protection, and it is the defined as the ratio between the mean energy $d\bar{\varepsilon}$ imparted to matter of mass dm by ionizing radiation [1]**Errore. L'origine riferimento non è stata trovata.**.

$$D = \frac{d\bar{\varepsilon}}{dm} \qquad \text{Eq. 1}$$

The SI unit of the absorbed dose is $\frac{J}{kg}$, which is also defined as Gray (Gy).

When using the quantity absorbed dose in practical radiation protection applications, doses are averaged over tissue volumes. It is assumed that, for low doses, the mean value of absorbed dose averaged over a specific organ or tissue can be correlated with radiation detriment for stochastic effects in that tissue with an accuracy sufficient for the purpose of radiological protection. The averaging of absorbed dose ($D_{T,R}$ average absorbed dose in the volume of a specified organ or tissue T due to radiation of type R) is carried out over the mass of a specified organ, tissue or sensitive region of a tissue.
The equivalent dose is the one used as protection quantity in an organ or tissue and it is defined as the sum of the averaged absorbed doses times the weighting factors for radiation R (w_R), over all types of radiation involved [1].

$$H_T = \sum_R w_R \cdot D_{T,R} \qquad \text{Eq. 2}$$

The unit of equivalent dose is $\frac{J}{kg}$ and has the specific name Sievert (Sv).

The effective dose E is defined by a weighted sum of tissue equivalent doses as follows:

$$E = \sum_T w_T \cdot H_T = \sum_T w_T \cdot \sum_R w_R \cdot D_{T,R} \qquad \text{Eq. 3}$$

The values of w_T are the weighting factors for tissues and the sum is equal to 1; they are chosen to represent the contributions of individual organs and tissues to overall radiation detriments from stochastic effects. The unit of the effective dose is again Sv.
Another important parameter that will be used in this analysis is the Kerma (K), which represents the quotient of the sum of the kinetic energies, dE_{tr}, of all charged particles (e.*g.* electrons) liberated by uncharged particles (*e.g.* photons) in a mass dm of material, and the mass dm of material.

$$K = \frac{dE_{tr}}{dm} \qquad \text{Eq. 4}$$

Kerma is defined as a non-stochastic quantity and the unit is Gy [1].

The body-related protection quantities are not measurable in practice and therefore cannot be used directly as quantities in radiation monitoring. Operational quantities are, therefore, used for the assessment of effective dose or equivalent doses in tissues or organs. They are aimed at providing an estimate or upper limit for the value of the protection quantities related to an exposure, or potential exposure of people under most irradiation conditions.
Operational dose quantities are used because instruments for radiation monitoring need to be calibrated in terms of a physical quantity for which calibration standards exits.
The ICRU (International Commission on Radiation Units & Measurements) stated that $H_p(10)$, defined as the dose equivalent at a body depth of 10 mm at the point of application of the personal dosimeter, is designed for monitoring strongly penetrating radiation (photons above 12 keV and neutrons), while $H_p(0.07)$, dose equivalent at a body depth at 0.07 mm, is applied for low-penetrating radiation (beta particles).
The assessment of doses from exposure to radiation from external source is usually performed by individual monitoring using personal dosimeters worn on the body. The operational quantities for individual monitoring are $H_p(0.07)$ and $H_p(10)$. If the personal dosimeter is worn on a position of the body representative of its exposure, at low doses and under the assumption of a uniform whole-body condition, the value of $H_p(10)$ provides an effective dose value sufficiently precise for radiological protection purpose.
As already said the protection quantities, equivalent dose and effective dose, are not measurable and their values are assessed using their relationship to either radiation field quantities (air Kerma free in air K_a), or particle fluence ϕ, or operational dose quantities. In order to provide a practicable approach, these coefficients are calculated for standard conditions (monoenergetic radiations, standard irradiation geometries) in anthropomorphic phantoms with clearly defined geometries, which include most organs and tissues in the body. In case of photons the parameter taken into consideration is the air Kerma, in fact the conversion coefficient reported are the absorbed dose in an organ or tissue per air Kerma free in air and the effective dose per air Kerma free in air [1].

The annual regulatory limit of the effective dose for the public is of 1 mSv, while for occupational exposure the limit is 20 mSv (averaged over defined periods of 5 years). Concerning the annual equivalent dose, limits are subdivided considering the different parts of the body: eye lens, skin, hands and feet. For the public only eye lens and skin are considered and the limits are respectively of 15 and 50 mSv; workers' dose instead has to be lower than 150 mSv for eye lens, 500 mSv for skin, hands and feet [1].

Most adverse health effects of radiation exposure may be grouped in two general categories:

- *deterministic effects* like cataracts;
- *stochastic effects* i.e. cancer and heritable effects involving either cancer development in exposed individuals owing to mutation of somatic cells or heritable disease in their offspring owing to mutation of reproductive (germ) cells.

The effective dose is used as an estimator of the increased risk of develop stochastic effects due to exposure to ionizing radiation.

Cataract is the principal pathology of the lens, consisting on their opacification. The lens of the eye is one of the most radiosensitive tissues in the body; detectable lens changes are noted at doses between 0.2 and 0.5 Gy, while other ocular pathologies can be seen in cases of exposures between 5 and 20 Gy [2].

1.2 Occupational exposure of medical staff

For radiation protection purposes, occupationally exposed medical staff are required to wear a personal dosimeter that measures $H_p(10)$. Most whole-body personal dosimeters commercially available determine $H_p(10)$ through passive detectors sensitive to ionizing radiation, like Thermoluminescence (TL), Optically Stimulated Luminescence (OSL) or Radiophotoluminescence (RPL) dosimeters.

Figure 1. TL (left) [3], OSL (center) dosimeters from Landauer [4] and RPL (right) dosimeter from IRSN [5].

Radioprotective garments (RPG), like a lead apron and thyroid collar, play a very important role in the radiation protection of personnel in interventional radiology and cardiology departments. They are worn in examination rooms during radiological examinations and their specific function is to reduce the exposure of medical staff to ionizing radiation scattered in the patient and room equipment. Typically, in IR and IC the frontal part of the lead garment (LG) has a lead-equivalent thickness of 0.5 mm.

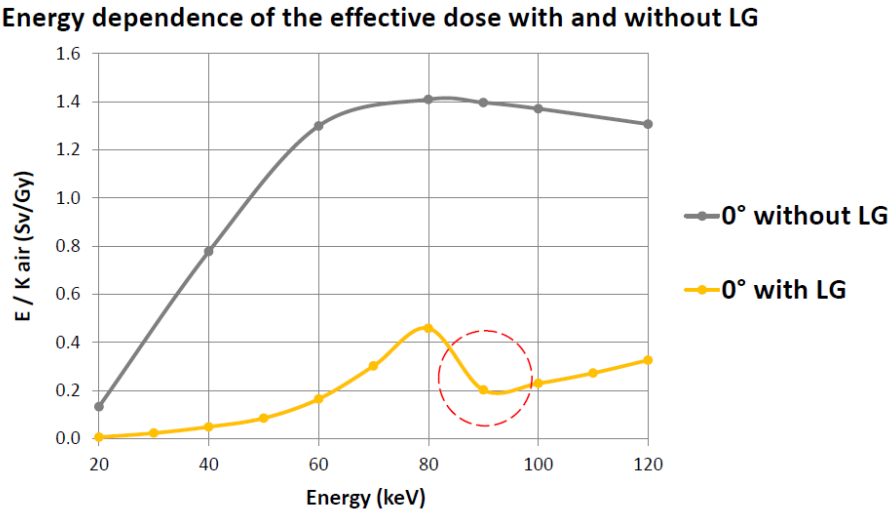

Figure 2. Energy dependence of the effective dose with and without radiation protection garments (obtained from previous studies at SCK•CEN.

Lead aprons are the most effective personal radiation protection means. They can reduce the dose received by $85 - 99\,\%$ depending in the energy of the X-rays (kV) and the lead equivalent thickness of the apron [6]. As shown in *Figure 2* the curve representing the effective dose received in presence of lead apron is always below the curve without shielding for all the range of energies considered: this means that lead can shield effectively scattered radiation in these exposure conditions. The decrease of the curve at 88 keV can be explained knowing the k-edge of lead. The k-edge is the binding energy of the K shell electron, closest to the nucleus. If photons with energy higher than the k-edge interact with the atom, there is a sudden increase in the attenuation coefficient of photons. This increase in the attenuation is due to photoelectric absorption of the photons and so, for energies higher than the binding energy of the electron, photons are more likely to be absorbed.
The body parts of the radiology operators receiving the main amount of dose are chest, hands, thyroid, legs and eyes.

1.3 Approaches to personnel dosimetry

There has been a continuing scientific debate about the personnel monitoring in interventional radiology [7]. The aim is to measure the effective dose through whole-body dosimeters, but sometimes is it necessary to evaluate also the maximum skin dose, which happens to be in the extremities, using ring dosimeters.
The evaluation of the effective dose, when RP garments are worn, is tricky. If a conventional $H_p(10)$ dosimeter is worn above the apron, there is an overestimation of the effective dose, the shielding is considered; while if located below, there is an underestimation because the exposure of non-protected parts like arms, head and legs is not taken into account.
This situation can cause potential worry for the individual monitored and avoidable problems for the personnel monitoring services concerned. So a careful estimate of the effective dose is fundamental because it allows an accurate estimation of risk.
A couple of personal dosimetry methodologies have been proposed to assess the effective dose of medical staff wearing radioprotective garments: single dosimetry and double dosimetry.

1.3.1 Single dosimetry

The approach of the single dosimetry (SD) involves the use of one single dosimeter worn over or under the RP garment and the successive modification of the measured personal dose equivalent through a correction factor, divider (D) or multiplier (M) depending on the location of the dosimeter.

$$D_{SD} = \frac{H_{over}}{D} \qquad D_{SD} = H_{under} \cdot M \qquad \text{Eq. 5}$$

Where H_{over} is the dose measured by the $H_p(10)$ dosimeter when it is worn over the apron, whereas H_{under} is the dose measured with the dosimeter worn under the apron.
The correction factors should generally be determined in an optimum way to minimize the underestimation of the effective dose. The methods based on the use of correction factors for a single dosimeter can result in significant errors because a single correction factor cannot account for the range of imaging conditions typically encountered in fluoroscopy [7].
Different correction factors have been proposed in case of single dosimetry. These factors are used to take into account the position of lead (above or below the dosimeter) and the presence or not of the thyroid collar [8].

Table 1. Comparison between different correction factors used in single and double dosimetry algorithms according to the studies performed [8].

COMPARISON OF DOUBLE DOSIMETRY ALGORITHMS

Table 1. Algorithms for the calculations of effective dose (E).

Double dosimetry algorithm	With TS		Without TS		Remarks
	α	β	α	β	
Wambersie and Delhove[8]	1	0.1	1	0.1	
Rosenstein and Webster[9]	0.5	0.025	0.5	0.025	
NCRP Report 122[10]	0.5	0.025	0.5	0.025	
Niklason *et al.*[11]	1	0.02	1	0.06	$H_o \rightarrow H_o - H_u$
Swiss Ordinance[12]	1	0.05	1	0.1	
McEwan[13]			0.71	0.05	
Franken and Huyskens[14]	1	0.033	1	0.1	
Sherbini and DeCicco[15]	1	0.07	1	0.07	
von Boetticher *et al.*[16]	0.65	0.017	0.65	0.074	
Lachmund[17]	0.65	0.017	0.65	0.074	
Clerinx *et al.*[18]	1.64	0.075	1.64	0.075	

Single dosimetry algorithm	With TS	Without TS	Remarks
	γ	γ	
NCRP Report 122[10]	21	21	
Huyskens *et al.*[19]	5	5	or $E = 3H_u$
Padovani *et al.*[20]	33	14	assuming $H_u \sim 0.01H_o$
McEwan[13]		12.5	

TS: thyroid shield.

Single dosimeter worn under radiation protection garments shouldn't be used because it provides no information about eye radiation and doesn't account for contribution of organs and tissues not covered by a protective garment, giving as result an underestimation of the effective dose. Instead, if a single dosimeter is worn over the garment, the effective dose will be overestimated due to the fact that the protective lead is not taken into account [8].

1.3.2 Double dosimetry

Double dosimetry (DD) consists on an algorithm combining the dose evaluated by two dosimeters, one worn above the protective garment (usually at chest/shoulder level or at the collar) and one below (usually at the waist). For the evaluation of the correction factors and the constants, the presence of the thyroid collar has to be considered but the evaluation is independent from the lead apron thickness.

Several DD algorithms have been proposed, some of them were based on the effective dose and the others (the most recent ones) on the effective dose equivalent, and so considering the tissues weighting factors [8].

The use of a two-dosimeter monitoring system is more complicated in practice and requires the use of formulae that link the two doses, increasing the uncertainty of the results.

For these reasons, it is still not possible to obtain an acceptable estimation of the effective dose with radioprotective garments [9].

Table 2. Table of comparison between different double dosimetry algorithms and correction factors [10].

DOUBLE DOSIMETRY FOR RADIOLOGY

Table 1. Algorithms for the calculations of effective dose (E).

	Authors	Algorithm	Place of dosemeters	Remarks
1	Wambersie and Delhove[15]	$E = H_u + 0.1H_o$	H_u: chest H_o: neck or shoulders	
2	Rosenstein and Webster[16]	$E = 0.5H_u + 0.025H_o$	H_u: waist H_o: neck	Based on Faulkner and Marshall[14]
3	NCRP Report No. 122[5]	Single: $E = H_o/21$ Double: same as No. 2	H_o: neck	Based on data published until (including) 1993
4	Huyskens *et al.*[17]	Single: $E = H_o/D$ or $E = H_uM$		$D = 5$ and $M = 3$ for fluoroscopic interventional practice
5	Niklason *et al.*[8]	(a) Without TS, double: $E = 0.06(H_{os} - H_u) + H_u$ Single*: $E = 0.07H_{os}$ (b) With TS, double: $E = 0.02(H_{os} - H_u) + H_u$ Single*: $E = 0.03H_{os}$	H_u: waist H_{os}: collar	*Recommended by Padovani *et al.*[21]; assuming $H_u \sim 0.01H_{os}$ Tested by Mateya and Claycamp[19] and Kicken *et al.*[20]
6	Swiss ordinance[7]	$H_p(10) = H_u + \alpha H_o$ $\alpha = 0.1$ without TS $\alpha = 0.05$ with TS $H_p(0.07) = H_u + H_o$	Not defined	Without TS same as No.4.
	McEwan[22]	Double: $E = 0.71H_u + 0.05H_o$ Single: (a) $E = 0.08H_o$; (b) $E = 2H_u$	H_u: trunk H_o: collar	Without thyroid shield. Based on $E/H_p(10)$ ratios for AP exposures published by NRPB[30]
8	Franken and Huyskens[23]	Single: $E \leq H_o/5$ (a) Double without TS: $E \leq H_u + H_o/10$ (b) Double with TS: $E \leq H_u + H_o/30$	H_o: mid front (1) H_u: mid front (2) H_o: mid front (3) See →	Lead apron: at least 0.25 mm lead (1) At collar or chest level (2) At waist level (3) At collar level
9	Sherbini and DeCicco[24]	$E = 1.0H_u + 0.07H_o$	H_u: waist H_o: neck	
10	von Boetticher *et al.*[25] and Lachmund[26]	(a) Double without TS: $E = 0.65H_u + 0.074H_o$ (b) Double with TS: $E = 0.65H_u + 0.017H_o$	H_u: anterior thorax H_o: neck	
11	Clerinx *et al.*[29]	$E = 1.64H_u + 0.075H_o$	H_u: thorax H_o: neck	Estimation within a 10% underestimation margin

Symbols: H_u: under apron dose, H_o: over apron dose, E: effective dose[13], H_{os}: overcollar shallow dose, i.e. $H_p(0.07)$, TS: thyroid shield.

1.4 Purpose of the project

The aim of this project is to design a new whole-body dosimeter suitable for estimating the effective dose of IR/IC medical staff wearing RPG. The dosimeter would be worn above the RP apron and should estimate the effective dose with RP garments more accurately than the already existent personal methods. The design of this dosimeter should be such that its energy and angular response $D_{dosimeter}(E_{photon}, \phi)$ is as similar as possible to that of the effective dose with 0.5 mm lead garments $E_{RP-garments}(E_{photon}, \phi)$, *i.e.*, the ratio between $D_{dosimeter}$ and $E_{RP-garments}$ should be al close as possible to one for all photon energies and angles of incidence in the range of interest in IR and IC applications.

Different factors determine the characteristics of the dose response of the dosimeter for given exposure conditions: type of the dosimetric detectors (intrinsic dose response, material composition and geometry), components around the detectors (filters, holders and support with all the information about material composition, geometry and position) and method used for the estimation of the dose (use of correction factors or algorithms). The optimization of the dose response of a dosimeter relies on the good selection and combination of these factors. A simplified model of such a dosimeter has already been designed at SCK•CEN using TL detectors of the type LiF:Mg,Ti. Starting from that simplified model, this project will focus on designing a dosimeter for the same application, but based on RPL glass detectors. The objective is to understand the strong energy dependence of the detector and modify the number, the dimensions and geometries, the materials and the structure of the filters inserted above and below it such that dose of the dosimeter is as close as possible to the effective dose with RPGs.

2. MATERIALS AND METHODS

The design of the new dosimeter has been performed by means of Monte Carlo simulations using a transport code under all possible exposure conditions of medical staff, concerning interventional radiology and cardiology. The simulations allowed to evaluate the absorbed dose (energy per unit mass) in the detecting volumes of the detector, considering firstly parallel and monoenergetic photon beams and then radiation qualities.
The results of the calculations have been converted into values of dose per air kerma, and combined with the purpose of comparing the final effective dose to the reference values of the effective dose with radiation protection garments, provided by previous analysis.

2.1 Effective dose with lead garments

The effective dose calculated with the RP garments will be used as reference for optimizing the energy and angular response of the dosimeter. For this purpose the ICRP reference computational male phantom has been equipped with a mathematically defined $0.5\ mm$ thick lead apron and thyroid collar and its effective dose has been evaluated through Monte Carlo simulations for photon beams with energies and angles of incidence in interventional radiology and interventional cardiology.
Effective dose with lead garments ($E_{RP-garments}$) per air kerma free in air (K_{air}) conversion coefficients have been provided for whole-body unidirectional photon beams with energies between 20 and 120 keV (monoenergetic) and also for the standard radiation quality spectra relevant in fluoroscopy and personal radiation protection (RQR series, narrow (N) and wide (W) spectra series).
At low energies, most of the photons are absorbed by the lead of the RP garments and so the effective dose is very low. The main contribution of the effective dose comes from organs located in regions of the body, which are not covered by the garments. As the photon energy increases, more photons start traversing the barrier of lead and so the effective dose increases steeply. All organs relevant for the effective dose calculation contribute until 88 keV, when photons reach the energy of the K-absorption edge of lead and the effective dose suddenly decreases. Above 88 keV the effective dose starts to increase again with the photon energy but remains lower than the dose reached just below the K-edge, for photon energies lower than 120 keV.
For photon beams parallel to the transversal plane, when the angle of incidence increases (regardless of the sign), the effective dose increases or decreases depending on the energy of the photon beam.
Concerning photon beams parallel to the sagittal plane, the effective dose decreases strongly when the angle of incidence increases; this is related to the geometry of the RP garments. In the sagittal plane the effective thickness of lead that photons need to

penetrate to reach body tissues is higher as the angle of incidence increases due to the flat geometry of the garments. Therefore, as the angle of incidence increases on the sagittal plane, less radiation passes through the lead garments and the effective dose becomes lower [11].

The coefficients of the effective dose E_{apron} per incident air Kerma (K_{air}) are shown in the figures for different photon beam energies and angles of incidence.

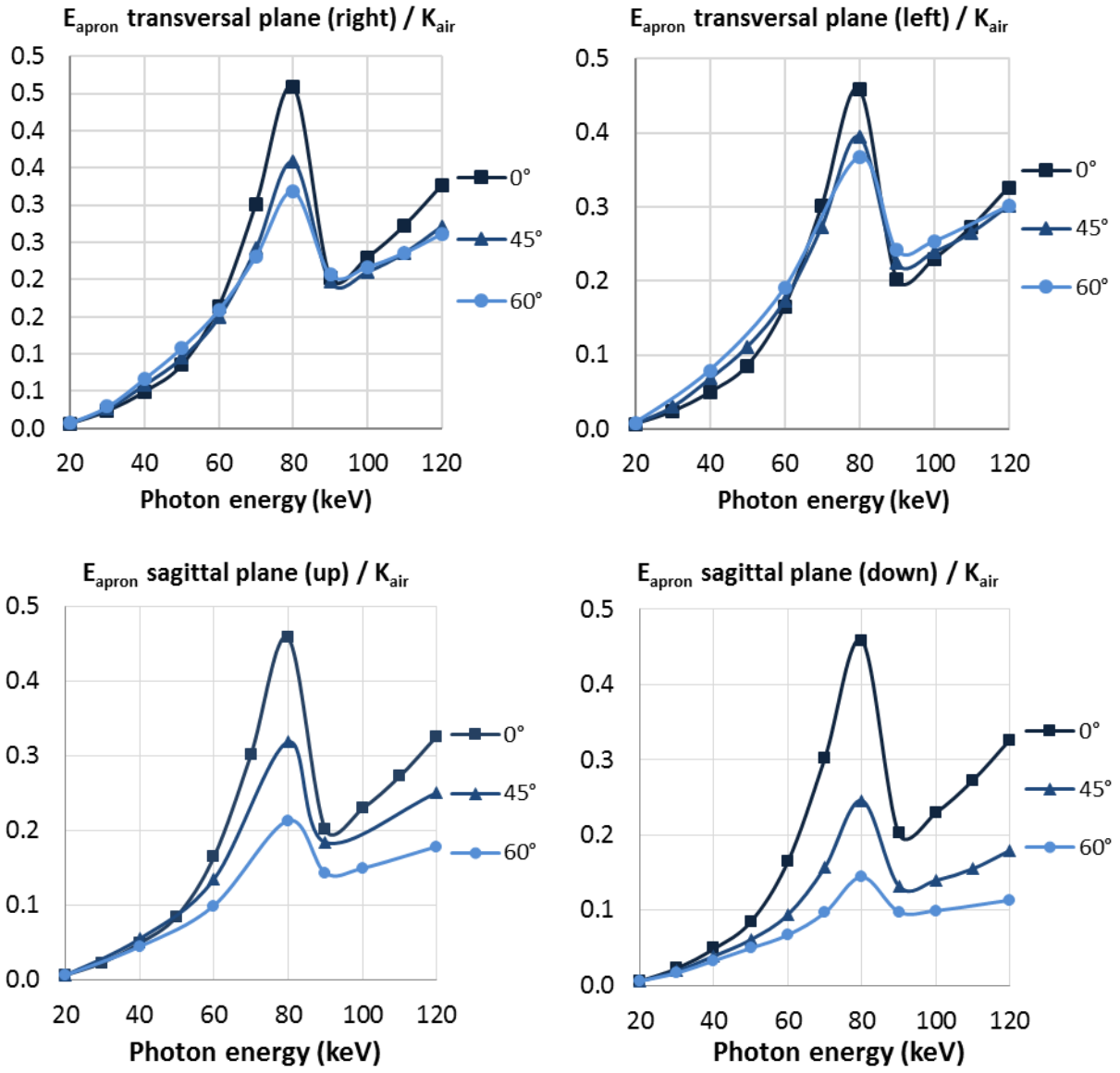

Figure 3. Effective dose per air Kerma for different values of photon energy and angles of incidence. In this graphs, beams in the transverse plane coming from the right direction (top left) and from the left (top right), beams in the sagittal plane coming from up (bottom left) and down(bottom right) are shown [11].

2.2 Dosimeter

The first part of the analysis consisted in the modification of the dosimeter previously designed at SCK•CEN using TL dosimeters. The geometries and the materials of such dosimeter model are shown in *Figure 4*.
As already introduced, the innovative idea is to use only one dosimeter worn over the apron.

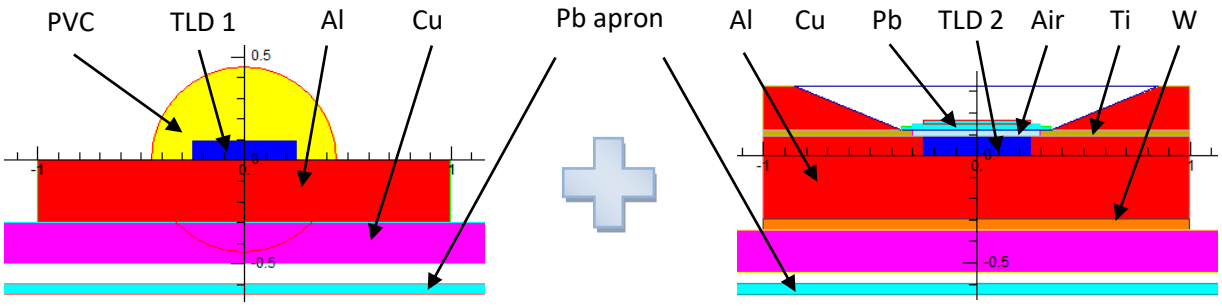

Figure 4. Simplified geometry made be two separate TL dosimeters with low Z materials filtration (left) and high Z materials filtration (right) [11].

The simplified model has been constructed in order to study separately the responses of two detectors when different kinds of filtration are present above and below them.
Low Z materials filtration is necessary to reproduce the condition of dose received by parts of the body not covered by RP garments, while high Z materials filtration allows to evaluate the dose received by the parts of the body covered by radioprotective garments.
The combination of these two dose values through the algorithm gives an estimation of the effective dose and appropriate constants are used to provide values as close as possible to the reference values.

The results of the simulations, obtained through the tally, have to be divided by the corresponding value of air Kerma, relative to the energy and the angle of the photon beam. At this stage, the values of doses per air Kerma are used for the evaluation of the combined dose according to the following algorithm:

$$D_{combined} = \alpha \cdot (D_2 + \beta \cdot D_1) \qquad \text{Eq. 6}$$

The effective dose can't be measured directly. For this reason air kerma, which is a measurable quantity outside the human body, has been calculated by previous SCK•CEN studies and provided. By using the tissue weighting factor, the estimation of the dose equivalent and effective dose is possible. Correction factors are provided to the values of effective dose per air kerma free-in-air, depending on the energy of the photon beam and its angle of incidence [12].

D_1 is the dose evaluated under the low Z filter geometry, D_2 is the dose under the high Z filter geometry, while α and β are appropriate constants identified arbitrarily.
The final step consists in the comparison between the combined dose per air kerma and the effective dose per air kerma already evaluated using ICRP voxel phantom with 0.5 mm of lead apron. The aim is to have the ratio $D_{combined}/E_{RP\text{-}garment}$ equal to one for all the incident photon beams and for all the energies considered, reducing the underestimations and the overestimations.

Low and high Z filtration materials are determined looking at the different chemical and physical characteristics, like the atomic number (Z), the attenuation coefficient and the density. The choice of the right values of these parameters enables the estimation of the thicknesses of the materials that best satisfy the requests of the various types of shielding.
A narrow beam of monoenergetic photons with an incident intensity I_0, penetrating a layer of material with mass thickness x and density ρ, emerges with intensity I given by the exponential attenuation law:

$$\frac{I}{I_0} = e^{-\frac{\mu}{\rho}\cdot x} \qquad \text{Eq. 7}$$

This equation can also be written as:

$$\frac{\mu}{\rho} = \frac{1}{x}\cdot \ln\left(\frac{I}{I_0}\right) \qquad \text{Eq. 8}$$

and represents the value of the mass attenuation coefficient, which can be obtained from the measurement of the values of I, I_0 and x. The mass thickness is the results of the product between the real thickness t and the density ρ, $x = \rho \cdot t$ [13].
An important quantity to be considered is the Mass Energy-Absorption Coefficient, $\frac{\mu_{en}}{\rho}$, and it can be described through another parameter, called Mass Energy-Transfer Coefficient $\frac{\mu_{tr}}{\rho}$, which represents the product of the mass attenuation coefficient and the fraction of energy transferred to the charged particles as kinetic energy, by the interacting incident photons. That is the fraction f of the mass attenuation coefficient that produces kinetic energy for ejected electrons from their atomic shell. Thus, $\frac{\mu_{tr}}{\rho}$ takes into account the escape only of secondary photon radiations produced at the initial photon-atom interaction site, plus the quanta of radiation from the annihilation of positrons originating in the initial pair production interactions. The Mass Energy-Absorption Coefficient involves the further emission of radiation produced by the charged particles travelling through the medium and it is correlated to the Mass Energy-Transfer Coefficient by the relation:

$$\frac{\mu_{en}}{\rho} = (1-g)\cdot\frac{\mu_{tr}}{\rho} \qquad \text{Eq. 9}$$

The factor *g* represents the average fraction of the kinetic energy of secondary charged particles (produced in all types of interactions) that is subsequently lost in radiative (photon-emitting) energy-loss processes as the particles slow to rest in the medium. The evaluation of *g* is accomplished by integrating the cross section for the radiative process of interest over the differential track length distribution established by the particles in the course of slowing down [14].

The following graphs present the values of the mass attenuation coefficient and the mass energy-absorption coefficient for some among the most relevant materials.

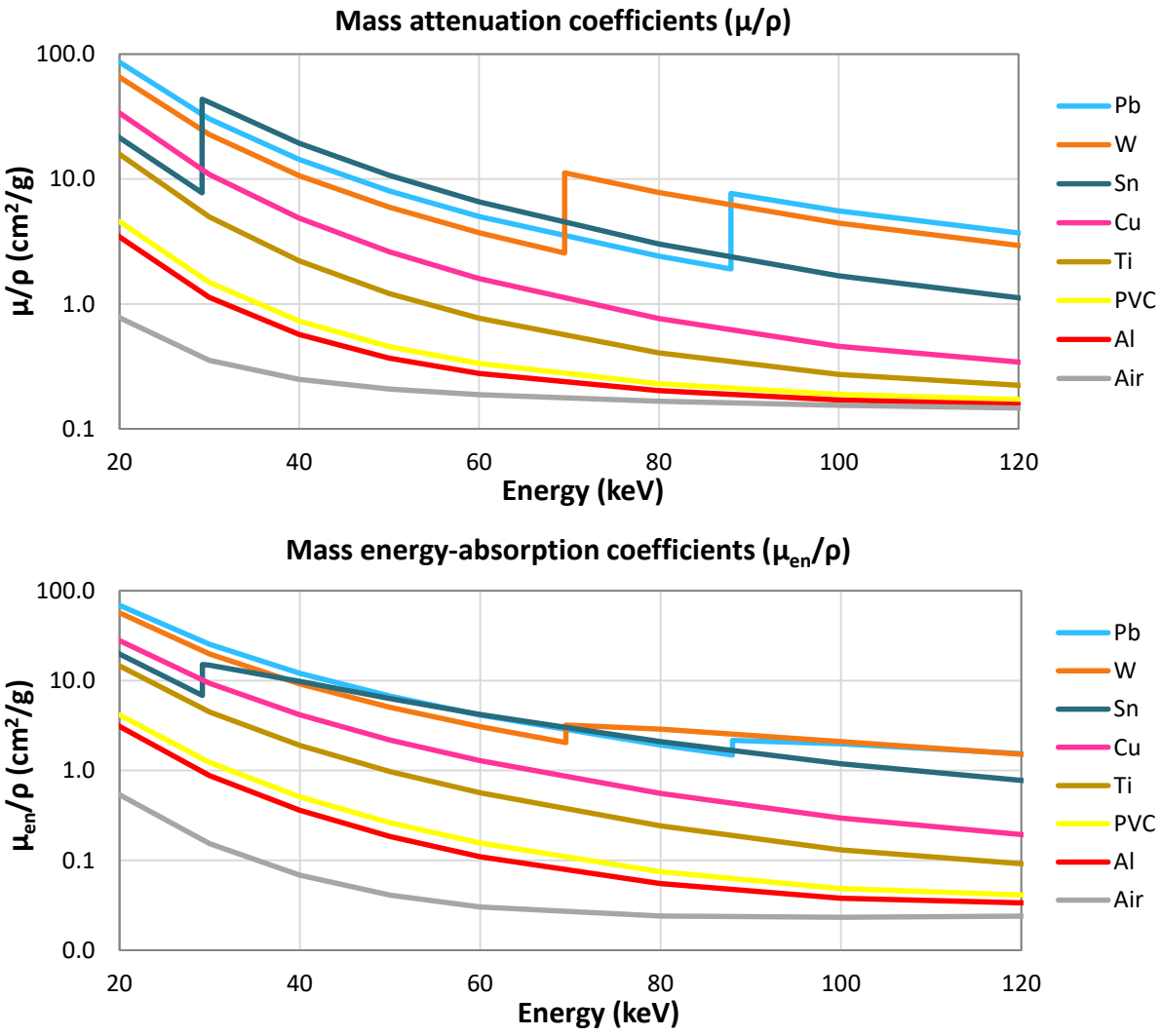

Figure 5. Mass attenuation coefficients (top) and mass energy-absorption coefficients (bottom) for different filtration materials.

2.2.1 Simplified dosimeter

The first simplification for the beginning of the project has been to examine separately the two configurations, without taking into account the plastic badge present around the detector, and consequently neglecting the problems related to dimension limits normally present in a dosimeter with a realistic geometry.
The detector, in this initial case still with dimensions and geometry of a TLD dosimeter, has a cylindrical shape with height of 0.1 cm and radius of 0.25 cm but the chemical composition has been changed to that of RPL glass (model GBF-J01 produced by Chiyoda Technol Corporation, Japan) [15].
The glass detector is formed by:

- $31.55\ \%\ P$
- $51.16\ \%\ O$
- $6.12\ \%\ Al$
- $11.00\ \%\ Na$
- $0.17\ \%\ Ag$

The environment around the dosimeter is considered void because the difference in terms of density and photon transport with respect to the air is not influencing considerably the results and it also reduced the computational time of the code.
For all the analysis only the lead apron shielding is considered, represented as a flat shield of thickness 0.05 cm and dimension of 10x10 cm^2 (reduced dimension with respect to reality).

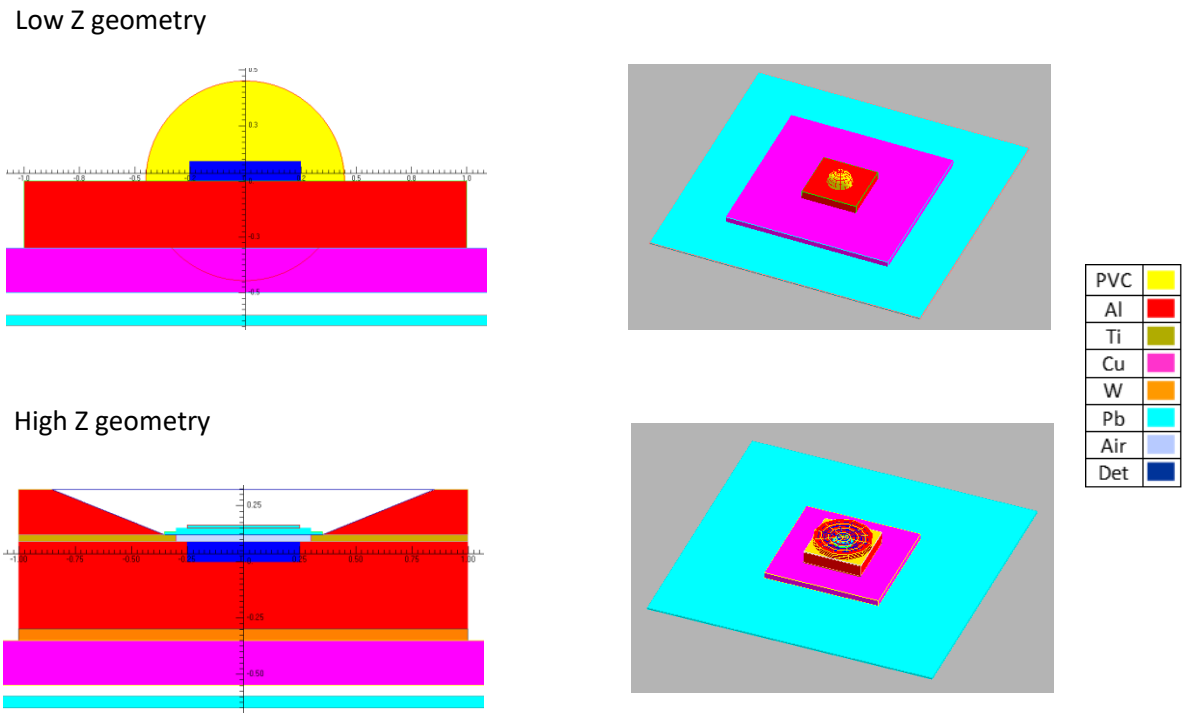

Figure 6. Initial configuration with RPL: low and high Z geometries (left) with the corresponding 3D representation (right).

2.2.2 Realistic dosimeter

The second part of this study focused on designing the RPL dosimeter using a more realistic geometry. The dosimeter presented in the paper of *Hocine et al* "Personal monitor glass badge: theoretical dosimeter response calculated with the Monte Carlo transport code MCNPX" (*Figure 7*) has been used as a starting point to design the new dosimeter.
With respect to the simplified dosimeter, the realistic one takes into account the real dimensions of the RPL dosimeter with the introduction of the ABS plastic badge. The detector inside the dosimeter has no more a cylindrical shape but it is represented by a parallelepiped (3.5x0.7x0.1 cm^3) [15].
Contrarily to the simplified geometry the detector is only one and up to now the number and the dimensions of the detecting volumes are unknown.

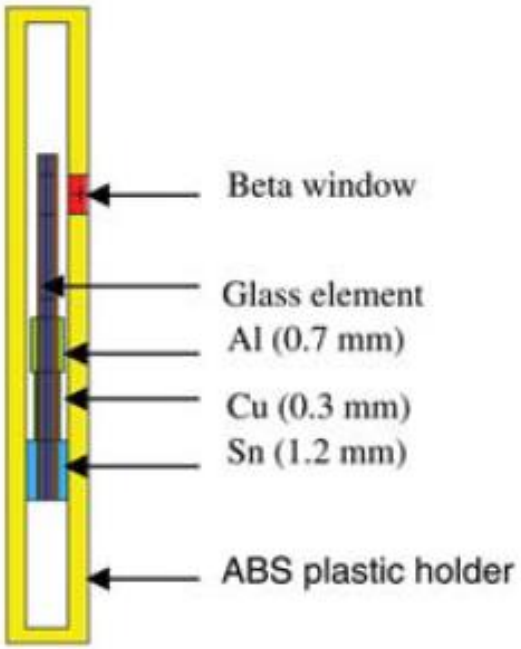

Figure 7. RPL geometry from the paper of Hocine et al. [15].

Such dosimeter consists of a plastic badge (6.1x3.0x0.8 cm^3) equipped with four filters composed of aluminium, copper, tin and plastic. This badge permits the measurements of the operational quantities $H_p(0.07)$ and $H_p(10)$.
The starting geometry designed as initial configuration is inserted below in *Figure 8*.

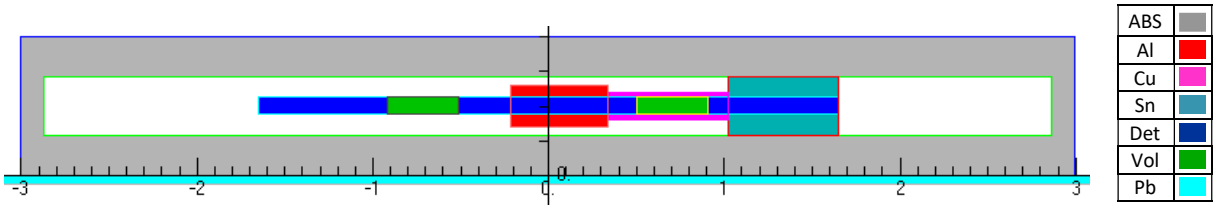

Figure 8. Starting design of the RPL geometry from the paper of Hocine et al.

It consists on an ABS plastic rectangular badge that covers the glass element. Three filters are inserted inside, and they have a ring shape such that they encircle the glass element. The filters are made by metals: aluminium (Al), copper (Cu) and tin (Sn). The green elements represent the detection points that will be used for the analysis.
The configuration just illustrated has been improved including the plastic support at the basis of the detector, the beta window, the five detection points of the detector in order to represent as better as possible the realistic structure of the dosimeter produced by IRSN (Insitut the Radioprotection et de Sûreté Nucléaire).

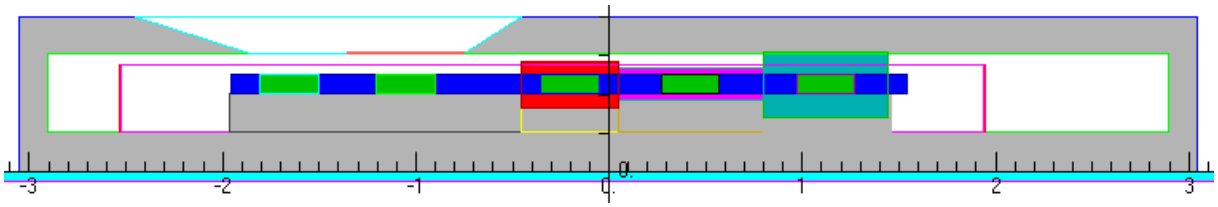

Figure 9. Starting design of the RPL geometry according to the prototype of IRSN provided.

The last step consisted in modifying the detection points according to the paper of *Maki et al*. "Development of the new glass badge". The RPL measurement volumes have the dimension of 0.17x0.3x0.05 cm^3 and are placed in the centre of each filter [16].

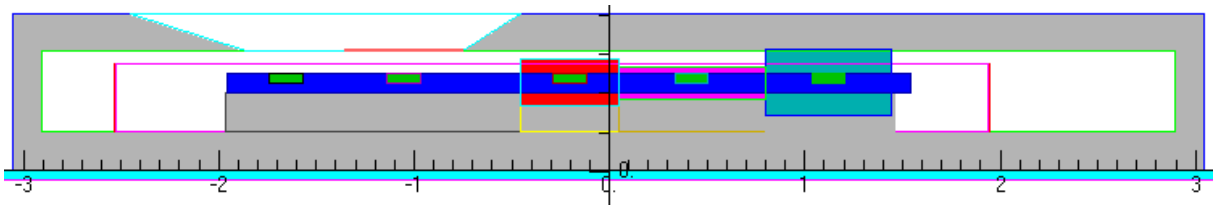

Figure 10. Starting design of the RPL geometry from the paper of Maki et al.

The last badge, which has been represented, is the one produced by Chiyoda Corporation since year 2000. This dosimeter presents a few differences with respect to the IRSN one, but for the purpose of this project, they will not be taken into account.

2.3 Exposure conditions

The aim of the simulations is to represent as much as possible the irradiation conditions that medical staff receives during the treatments of patients. For this purpose, the first step has been considering parallel monoenergetic beams of photons at ten different energies: 20, 30, 40, 50, 60, 70, 80, 90, 100, 120 keV. Once obtained a design of a dosimeter that allows an acceptable estimation of the effective dose with monoenergetic beams, the subsequent step has been performing the same analysis but taking into account the spectra provided. Three kinds of radiation qualities have been simulated: N, W spectra of ISO standard 4037-1 [17] and RQR spectra from IEC standard 61267 [18]. They have been selected with the purpose of covering the energy range mentioned above: N-30, N-40, N-50, N-60, N-80, N-100, N-120, W-60, W-80, W-110, RQR2, RQR4, RQR6, RQR7, RQR8, RQR9. For the graphical representation, the mean energy has been chosen for each case (*Table 3*).

Table 3. Mean energy of the radiation qualities considered.

Quality	Tube voltage (keV)	Mean energy (fluence) (keV)
N-30	30	24.3
N-40	40	32.9
N-60	60	47.5
N-80	80	64.8
N-100	100	83
N-120	120	100.4
W-60	60	44.6
W-80	80	56.5
W-110	110	79.1
RQR2	40	28
RQR4	60	36.4
RQR6	80	44.3
RQR7	90	48
RQR8	100	51.4
RQR9	120	57.4

As already introduced, two angles has been considered related to the respective planes: φ for the sagittal and ϑ for the transverse (*Figure 11*). The aim is to represent the real exposure of medical staff but for the beginning of the project only the transverse plane is analysed. Photon beams coming with angles of incidence of 0°, 45° and 60° with respect to the vertical axis have been analysed.

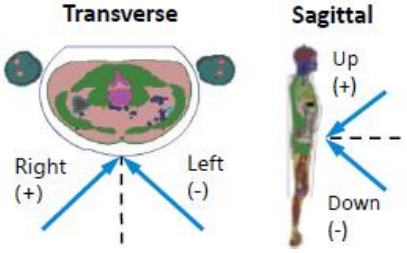

Figure 11. Transverse (left) and sagittal (right) planes with the angles of incidence of the photon beam.

Three graphs showing the energy dependence of the normalized frequencies of the radiation qualities cited above are reported.

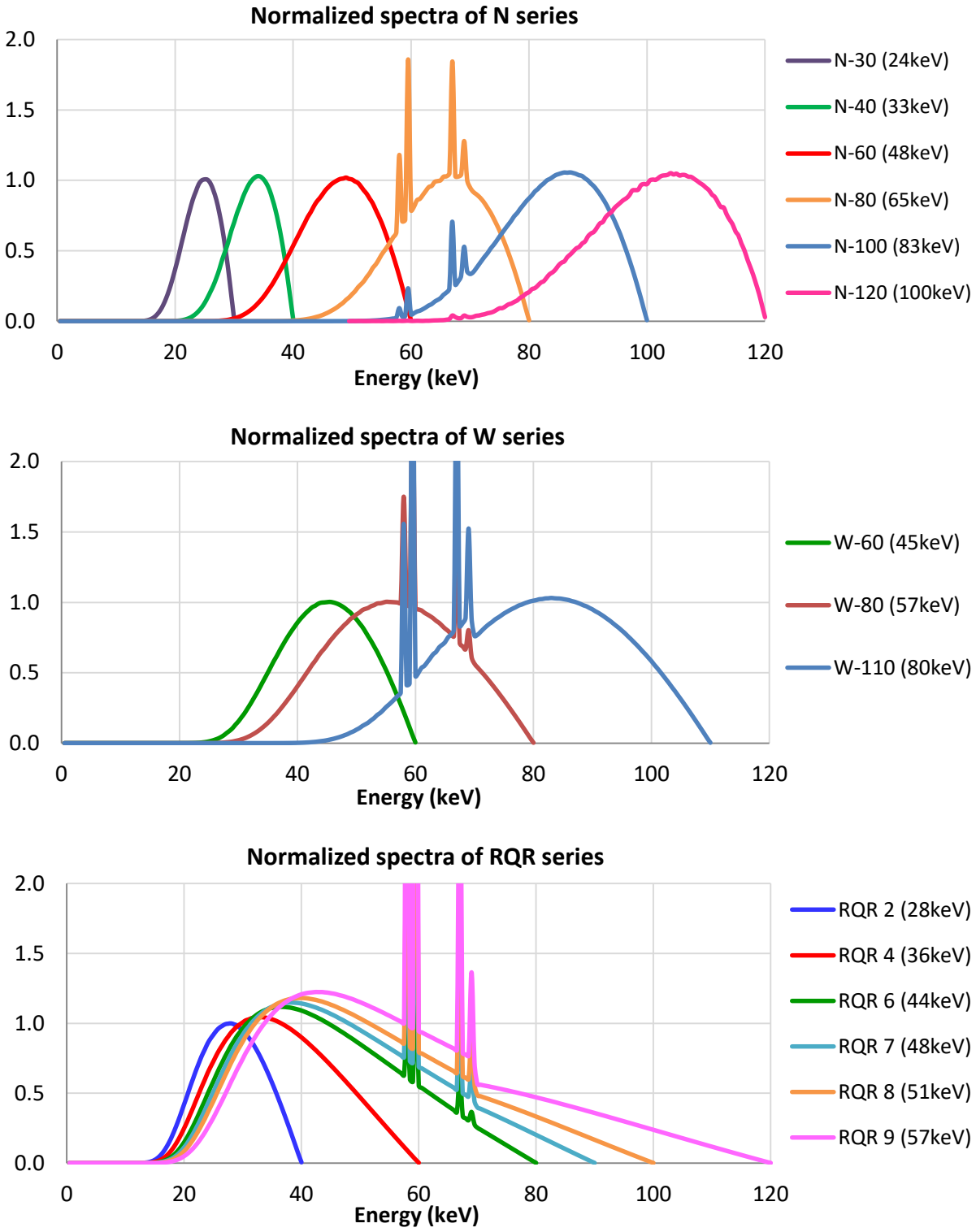

Figure 12. Normalized frequencies as a function of energy for N series (top), W series (middle) and RQR series (bottom).

2.4 Radiation transport

Interventional radiology (IR) refers to the techniques that rely in the use of radiological image guidance (X-ray fluoroscopy, ultrasound, computed tomography (CT) or magnetic resonance imaging) to precisely target surgery.
Interventional cardiology (IC) deals with treatments of structural heart diseases and uses again X-rays (fluoroscopy) for visualization.
The energy of the photons produced by the X-ray tube used in these kinds of procedures is normally below 120 keV. When radiation interacts with matter, energy is transferred to atoms and leads to excitation or ionization. Depending on the transmitted energy intensity, ionizing or non-ionizing radiation can be produced; ionizing radiation is often used in radiology and nuclear medicine and can be direct or indirect. Indirect ionizing radiation involves uncharged particles and they can either be absorbed or be scattered by atoms in matter. The frequency of the interaction of ionizing radiation with matter primarily depends on the type of material. As the atomic number increases, the frequency of interaction is higher. Energetic photons deposit energy in matter through the following processes: photoelectric effect, Compton effect and pair production. All three of these interactions result in the production of energetic electrons that, in turn, lose energy by exciting and ionizing target atoms and molecules and setting more electrons in motion.

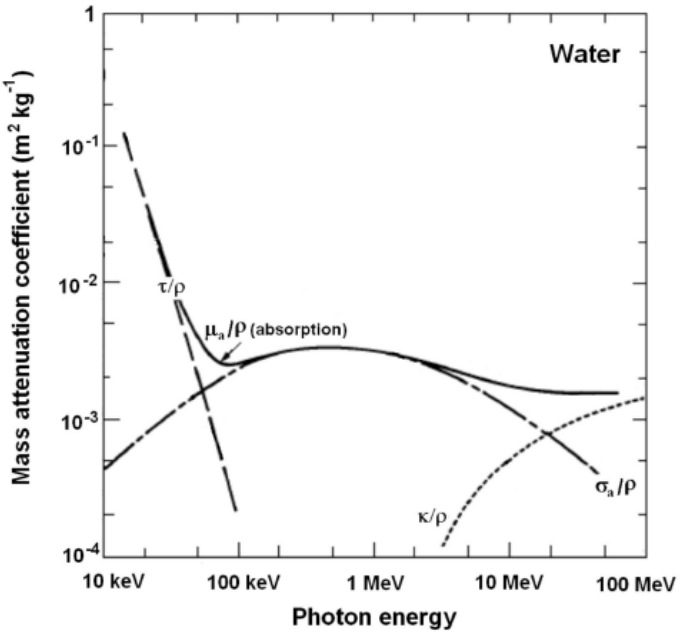

Figure 13. Mass attenuation coefficients as a function of the photon energy representing photoelectric, Compton and pair production effects [19].

- τ/ρ : photoelectric mass attenuation coefficient
- σ/ρ : Compton mass attenuation coefficient
- κ/ρ : pair production mass attenuation coefficient

The total mass energy absorption coefficient for water labelled μ_a/ρ reveals that only below 100 keV photoelectric processes are relevant. Compton scattering then dominates up to energies of a couple of MeV before pair production sets in. This implies that for the biologically most significant processes, Compton scattering and photoelectric effect are the dominant effects.

Photoelectric effect

The photoelectric effect describes the absorption of the incoming photon by an atom followed by the emission of a photoelectron under conservation of energy.

If an inner shell electron is removed, the respective vacancy is subsequently filled by an electron from a more loosely bound shell. Depending on the electron shells involved and on the Z of the atom, the excess energy is either emitted as a photon or released as kinetic energy of an electron.

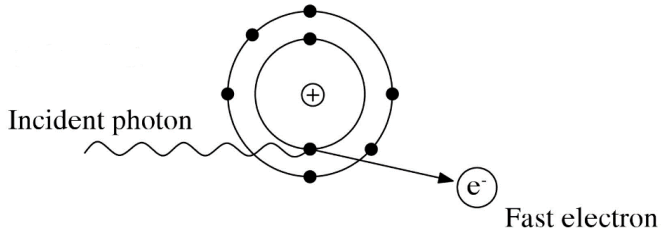

Figure 14. Simplified representation of the photoelectric effect [19].

Compton effect

In the energy range most widely used in radiotherapy (above 100 keV), the Compton effect is the most important mechanism leading to deposition of energy in a molecule. This energy-transfer process involves a photon scattering from a bound electron accompanied by momentum transfer to the electron. Because of the high photon energy, the bound electron can be considered "free". A broad spectrum of electron kinetic energies arises from Compton scattering which will cause the usual secondary processes.

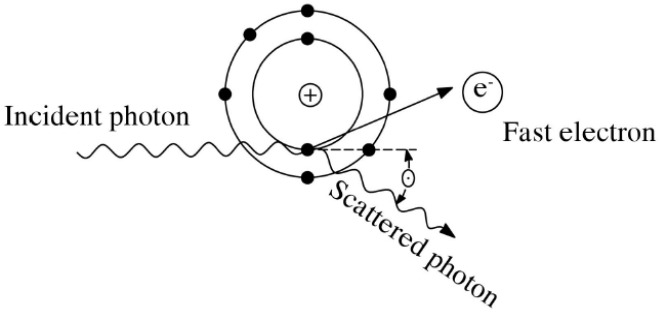

Figure 15. Simplified representation of the Compton effect [19].

In order to analyse the energy deposition in the new dosimeter, a Monte Carlo code has been used: MCNP code (Monte Carlo Neutral Particles), developed and maintained by Los Alamos National Laboratory. It the internationally recognized code for analysing the transport of neutrons, photons and electrons. The code deals also with coupled transport, i.e., transport of secondary gamma rays resulting from neutron interactions or transport of electrons, both primary source electrons and secondary electrons created in photon interactions [20].

High energy photons and charged particles interact with atoms primarily by producing excitations of the electron cloud, but this phenomenon has a negligible impact on the transport of photons and electrons. In each interaction, the primary photon is absorbed and in case of scattering, a secondary photon is reemitted.

The dominant interactions of electrons with atoms are elastic scattering, inelastic collisions and bremsstrahlung emission (radiation emitted when charged particles decelerate, for example when they hit a metallic target). Simulations with electron transport is more difficult with respect to photon transport only. The main reason is that the average energy loss of an electron in a single interaction is very small and so high energy electrons need a large amount of collisions before being slowed down.

In the simulations the MODE card, which allows to list all the particles that will be considered in the transport, has to be set. For the purpose of this problem, concerning photon exposure, *MODE p e* (photon and electron transport) has been chosen; this mode takes also into account the production and transport of secondary electrons. It is the most accurate model for physics treatment of photons but it is costly in terms of run time with respect to the simpler *MODE p*, in which electrons are created but immediately absorbed (kerma approximation) [21]. *MODE p* is not appropriate for the analysis because the assumption of considering only photon transport is not representing reality due to assumption that secondary photons and electrons are deposited locally. But for the purpose of the project, due to the presence of different layers of materials, their contribution has to be taken into account.

As it is a statistical based code, there are factors affecting the accuracy of the results, as explained in the MCNPX primer [20]:

- *The MCNP code* includes inaccuracies introduced by MCNP in its use of physics models, mathematical models, uncertainties in the nuclear/atomic data and coding errors.
- *The MCNP model* contains improper modelling of source energy and angular distributions, poor representation of the actual geometry by the MCNP geometric model and errors on the material compositions.
- *Users errors*, the most important sources of inaccuracies, are the errors induced by the user in incorrectly using the program options or making errors in the input file.

Another fact affecting precision is the number of histories performed; of course the more histories are run, the better will be the precision of the tallies in terms of statistics.

The main objective of using MCNP is to provide results with an acceptable relative error with the minimum computational time and cost. For this purpose, there are techniques called *variance reduction* that allow to reduce the relative error of a tally (or its variance) for a fixed computing time, or to decrease the computing time to achieve the same relative error.
Two approaches can be applied:

- simplify the MCNP model
- use non-analog simulations.

During non-analog simulations, very few of the source particles reach the detector or the region used for the tally. There is a way in which particles can artificially be forced to go towards specific regions, keeping the same input and getting the expected results. The idea is to assign each particle a weight such that the average of the particle weights reaching the detector is the same as in the true analog simulation.
The introduction of the importance card (IMP) permits to apply variance reduction techniques such as *geometry splitting* and *Russian roulette*.
In geometry splitting an *importance* is assigned to every cell; the general idea is to associate to the regions close to the tally a higher importance with respect to the further ones. When a particle leaves a cell with importance I_1 and enters a cell of importance I_2, the particle is split/rouletted according to the ratio ${I_2}/{I_1}$. For example if ${I_2}/{I_1} = 2.75$ the particle is split into 3 particles with 75% probability and into 2 particles with 25% probability; similarly if ${I_2}/{I_1} = 0.6$ the particle is killed with 40% probability and survive with 60% probability. In each splitting or Russian roulette, the weight of remaining particles is adjusted to leave the tally unbiased.
This technique of geometry splitting with Russian roulette is very reliable since, if no other biasing techniques are used, all the particles in a cell will have the same weight regardless of the paths taken to reach the cell [20].
The objective of the simulations is to estimate the dose read by the detector in the selected detecting volume. Once defined the cell of the measurement tally *F6: e* has been used to determine the energy deposition in that volume. The result provided by MCNPX is already in energy units $\left({MeV}/{g}\right)$ and it is normalized to one particle of the simulated source.
The result of the tally is then modified through the use of a multiplication card *FM*, with the aim of obtaining a value of absorbed dose in Gy.
The value reported as multiplication factor is the conversion from ${MeV}/{g}$ to Gy $\left({J}/{kg}\right)$ due to the relation $1\ MeV = 1.6022\ \cdot 10^{-13}\ J$.

$$1\left[\frac{Mev}{g}\right]\cdot 10^{3}\left[\frac{g}{kg}\right]\cdot 1.6022\cdot 10^{-13}\left[\frac{J}{MeV}\right] = 1.6022\cdot 10^{-10}\ Gy \qquad \text{Eq. 10}$$

3. RESULTS AND DISCUSSION

3.1 Simplified dosimeter

The first part of the analysis, as already introduced, consisted in a simplified dosimeter in which the configurations of the filters made by low and high Z materials have been studied separately. The choice of considering two different types of filtration is due to the impact they have on the shielding of the radiation and thus on the dose received by the dosimeter. Low Z filters (for example aluminium and PVC) act mainly on low energy photon beams because high energy photons are not influenced by them due to the lower probability of interaction, while high Z filters (for example lead and bismuth) shield almost all the low energy radiation and have their principal effect on high energies. The objective is to represent the irradiation conditions suffered by medical staff: low Z material filters represents the parts of the body which are not covered by radioprotective garments, while high Z filtration is introduced to take into account the contribution of organ and tissues located below the garments.

Starting from the dosimeter configurations for TLDs described before (*Figure 4*), simulations with monoenergetic photon beams have been performed in order to determine a geometry which allows an acceptable comparison between the combined dose evaluated and the reference values of effective dose provided, contemporary for 0°, 45° and 60° (angles of the photon beam in the transverse plane coming from the right direction).

The initial purpose has been to optimize the part of the dosimeter using low Z filters (i.e. part of the dosimeter with detector 1). Different materials and filter shapes were evaluated.

For each dosimeter configuration, $D_{combined}$ is computed and the results are compared with the effective dose with RPG. The PVC sphere, present in the original configuration (*Figure 6*), has been removed and substituted with other geometries. Among all the simulated models, ellipsoid, parallelepiped and truncated cone geometries are presented; actually different dimensions were tried for each shape but here only the ones that provided the most significant results in terms of angular dependence are reported.

To simplify the simulations for these following cases, *MODE p* has been used (i.e. transport of photons only). Thus, all electron energy is assumed to be deposited locally. Filters are made by materials with low Z and so only photon transport and deposition has been evaluated.

The environment of the dosimeter has been simulated as void. In the simplified dosimeter, the radiation detector is made by a cylinder of radius of 0.25 cm and height of 0.1 cm. The lead apron was modelled as a 10x10 cm^2 flat shield of 0.05 cm thickness and it will not be changed during all the following simulations concerning the simplified case and the realistic one.

3.1.1 Low Z filters

In this section three cases of different insertion of low Z filtrations in the dosimeter 1 are presented in *Table 4*, and then analysed and discussed. Only the shapes and the dimensions of the front filters have been modified, while the back filters made by parallelepipeds of aluminium and copper remain the same.

Table 4. Summary of the most relevant low Z filter configurations evaluated (i.e. filters around detector 1) for the simplified dosimeter. Front and back filters are reported with the corresponding shapes and dimensions.

CASE	FRONT FILTERS		BACK FILTERS	
	MATERIAL SHAPE	DIMENSIONS (cm)	MATERIAL SHAPE	DIMENSIONS (cm)
1A	PVC Ellipsoid	$a = 0.05$ $b = 0.05$ $c = 0.02$ $\frac{x^2}{a^2} + \frac{y^2}{b^2} + \frac{z^2}{c^2} = 1$	Aluminium Parallelepiped	$x = 2$ $y = 2$ $z = 0.3$
2A	PVC Parallelepiped	$x = 1$ $y = 1$ $z = 0.2$	Copper Parallelepiped	$x = 6$ $y = 6$ $z = 0.2$
3A	PVC Truncated cone	$r = 0.2$ $R = 0.4$ $h = 0.25$		

The responses of the detector with the different shapes show the strong energy dependence that affect the RPL dosimeters.

With respect to the configuration in absence of filters (*Figure 16*), the responses are less pronounced for low energies, which is due to the introduction of the PVC filter above that shield incoming photons at low energies. The presence of aluminium and copper is instead useful for attenuating the backscatter from lead.

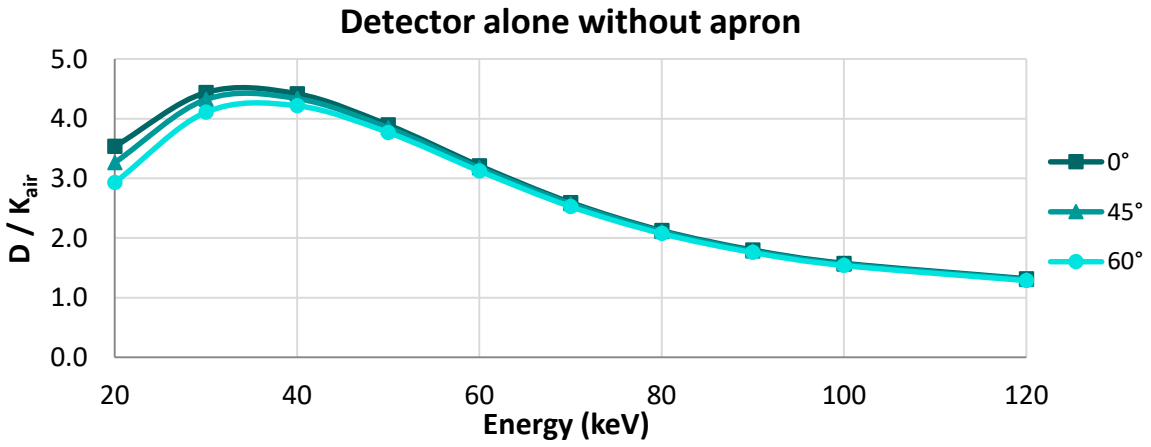

Figure 16. Response of the detector alone, without filters and lead apron.

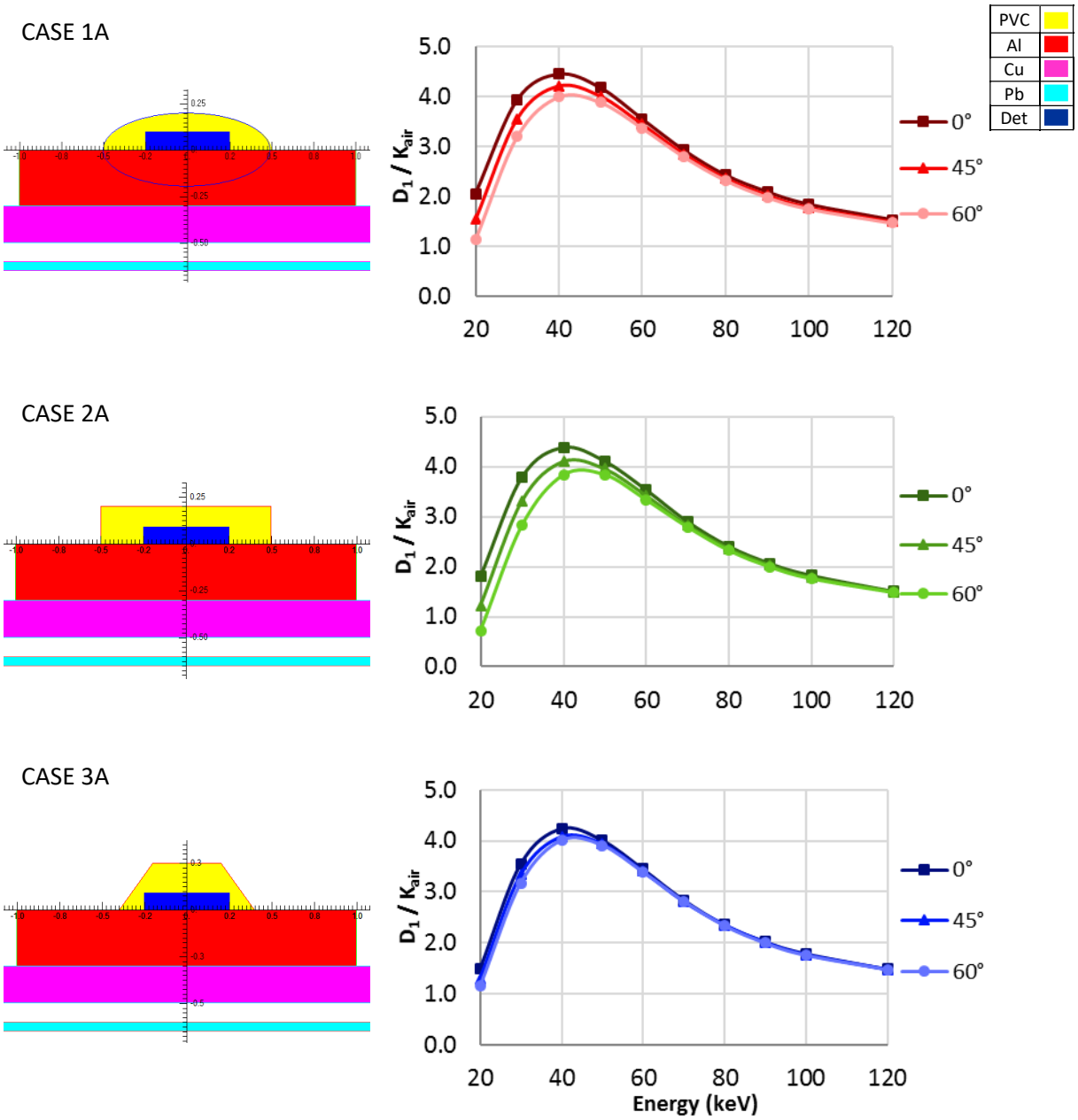

Figure 17. Low Z filter configurations and corresponding response of the dosimeter in terms of dose per air kerma for CASE 1A (top), CASE 2A (center) and CASE 3A (bottom).

The strong energy dependence of the RPL dosimeter is due to the chemical composition of the detector; conversely to TLDs, there is the presence of higher Z materials (for example P and Ag). The response of RPL dosimeter overestimates the true dose in the low energy range, however there is no problem at higher energies. This is due to photoelectric interaction of low energy with high effective atomic number elements within dosimeter which increases the dose response of the RPL dosimeter.

In order to see the effects of these three configurations, the doses read by the detectors as a function of the energy (keV) are shown together and compared (*Figure 18*).

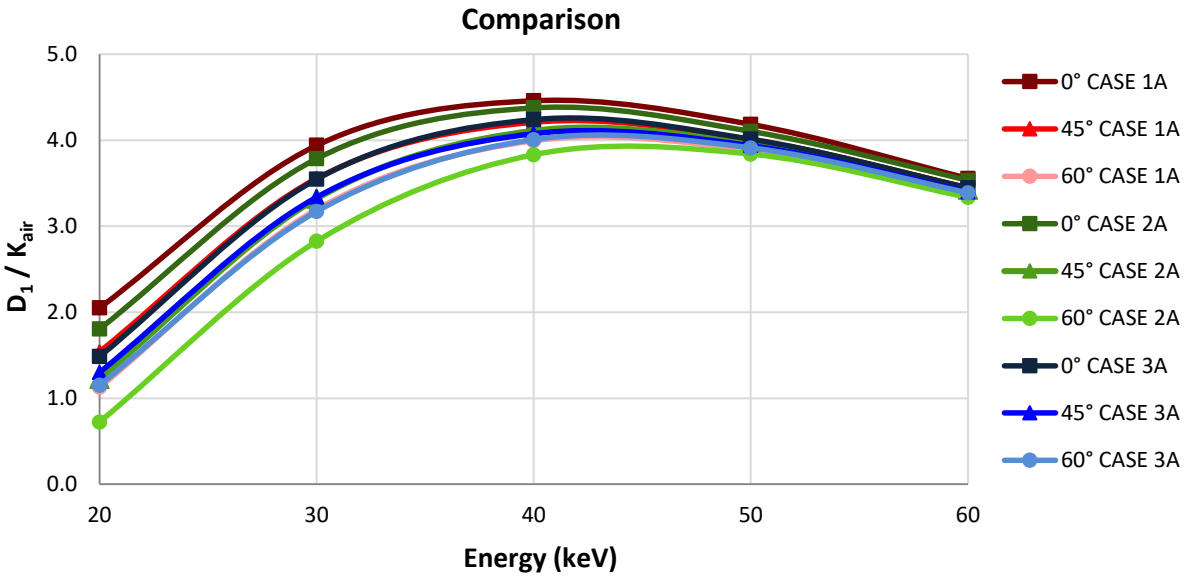

Figure 18. Comparison between the responses of the three simplified dosimeters when the shape of the PVC surrounding the detector is modified.

It is possible to notice how the low Z filters influence mainly the dose measured at low energies, keeping the higher energy responses almost unchanged.

This means that the PVC plastic filter, which is composed by hydrogen (~5%),carbon (~38%) and chlorine (~57%) and has a density of 1.4 $g \cdot cm^{-3}$, shields mainly low energy photons (20 – 30 keV) while high energy photons (40 – 120 keV) can reach the detector.

The curve of the attenuation coefficient of PVC, which represents the probability of interaction as a function of energy, shows a maximum at low energies and then it decreases continuously as the energy increases. This means that photons with low energies will undergo more interactions when penetrating PVC and so, they will be more attenuated in that region with respect to the one of higher energies.

Comparing the dose received by the detector in the configuration using an ellipsoidal filter (case 1A) with the effective dose, the results are high at low photon energies, which means that the filter used is not thick enough. Modifying the shape to a parallelepiped, it is evident that for the beam having an angle of incidence of 60° the attenuation is much higher with respect to the other angles, due to the presence of a greater amount of PVC in that angle of incidence, whereas the dose at 0° is the same for both cases. The shape of the truncated cone has been evaluated (case 3A) because the aim is to obtain a dose response with a weaker angular dependence: in this way the curves relative to the three angles considered almost overlap (lines represented by shades of blue in *Figure 17* at the bottom).

3.1.2 High Z filters

The objective of this subsection is to describe and analyse the dosimeter when high Z material filtration is introduced above and below the detector.
Four cases have been selected in order to reproduce in a consecutive way the main steps of the optimization.

Table 5. Table of comparison of the cases with high Z materials for the simplified dosimeter. Front and back filters are summarized with the corresponding shapes and dimensions.

CASE	FRONT FILTERS		BACK FILTERS	
	MATERIAL SHAPE	DIMENSIONS (cm)	MATERIAL SHAPE	DIMENSIONS (cm)
1B	Lead Cylinders (3)	$r_1 = 2$ $r_2 = 2$ $r_3 = 0.3$ $h_1 = h_2 = h_3 = 0.014$	Aluminium Parallelepiped	$x = 2$ $y = 2$ $z = 0.3$
	Aluminium Cylinder + Air gap Truncated cone	$r_{cylinder} = 1$ $h_{cylinder} = 0.2$ $r_{cone} = 0.35$ $R_{cone} = 0.85$	Tungsten Parallelepiped	$x = 2$ $y = 2$ $z = 0.8$
	Titanium Parallelepiped	$x = 2$ $y = 2$ $z = 0.3$	Copper Parallelepiped	$x = 4$ $y = 4$ $z = 0.2$
	Air gap Cylinder	$h = 0.03$ $r = 0.3$	-	-
2B	Bismuth (1) and lead (2) Cylinders	$r_1 = 2$ $r_2 = 2$ $r_3 = 0.3$ $h_1 = h_2 = h_3 = 0.014$	Aluminium Parallelepiped	$x = 2$ $y = 2$ $z = 0.15$
	Aluminium Cylinder + Air gap Truncated cone	$r_{cylinder} = 1$ $h_{cylinder} = 0.1$ $r_{cone} = 0.35$ $R_{cone} = 0.85$	Bismuth Parallelepiped	$x = 2$ $y = 2$ $z = 0.01$
	Titanium Parallelepiped	$x = 2$ $y = 2$ $z = 0.3$	Tungsten Parallelepiped	$x = 2$ $y = 2$ $z = 0.08$
	Air gap Cylinder	$h = 0.02$ $r = 0.3$	Copper Parallelepiped	$x = 4$ $y = 4$ $z = 0.2$

Table 5 (continuation). Table of comparison of the cases with high Z materials for the simplified dosimeter. Front and back filters are summarized with the corresponding shapes and dimensions.

CASE	FRONT FILTERS		BACK FILTERS	
	MATERIAL SHAPE	DIMENSIONS (cm)	MATERIAL SHAPE	DIMENSIONS (cm)
3B	Bismuth (1) and Lead (2) Cylinders	$r_1 = 0.35$ $r_2 = 0.30$ $r_3 = 0.25$ $h_1 = h_2 = h_3 = 0.014$	Aluminium Parallelepiped	$x = 2$ $y = 2$ z = 0.15
	Aluminium Cylinder + Air gap Truncated cone	$r_{cylinder} = 0.3$ $h_{cylinder} = 1$ $r_{cone} = 0.35$ $R_{cone} = 0.70$	Bismuth Parallelepiped	$x = 2$ $y = 2$ $z = 0.06$
	Titanium Parallelepiped	$x = 2$ $y = 2$ $z = 0.3$	Copper Parallelepiped	$x = 4$ $y = 4$ $z = 0.2$
	Air gap Cylinder	$h = 0.02$ $r = 0.3$	-	-
4B	Bismuth (1) and Lead (2) Cylinders	$r_1 = 2$ $r_2 = 2$ $r_3 = 0.3$ $h_1 = 0.024$ $h_2 = h_3 = 0.012$	Aluminium Parallelepiped	$x = 2$ $y = 2$ $z = 0.15$
	Aluminium Cylinder + Air gap Truncated cone	$r_{cylinder} = 0.3$ $h_{cylinder} = 1$ $r_{cone} = 0.35$ $R_{cone} = 0.75$	Bismuth Parallelepiped	$x = 2$ $y = 2$ $z = 0.03$
	Titanium Parallelepiped	$x = 2$ $y = 2$ $z = 0.3$	Copper Parallelepiped	$x = 4$ $y = 4$ $z = 0.2$
	Air gap Cylinder	$h = 0.02$ $r = 0.3$	-	-

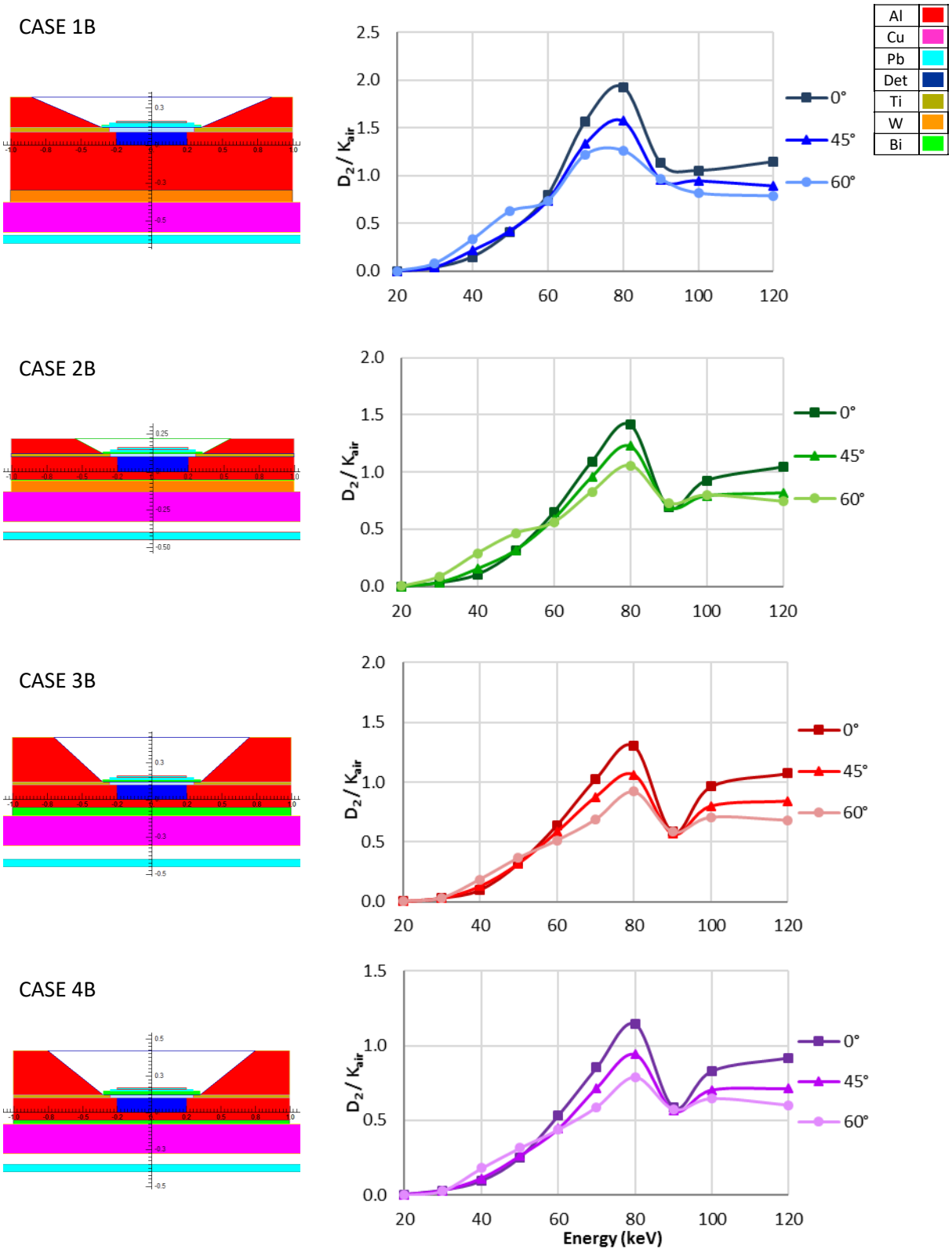

Figure 19. High Z filter configurations and corresponding response of the dosimeter in terms of dose per air kerma for cases 1B, 2B, 3B, 4B.

Figure 19 shows the configurations of the four dosimeters with the four different types of high Z filtration and their respective energy response under a monoenergetic photon exposure while *Table 5* is a summary of the characteristics of each filter, including the shape and the dimensions.

The best configuration will be selected through the comparison of the combined doses, which have been evaluated for every geometry applying the algorithm already described and the effective dose with lead garments.

Among the low Z geometries, only the one of the truncated cone (case 3A) will be used as D_1, while the values of D_2 will be all the ones described in cases 1B, 2B, 3B, 4B.

The ratio of $D_{combined}/E_{apron}$ has been calculated to evaluate the performance of each of the dosimeter configurations modelled and is shown in *Figure 20*, for different photon energies and angles of incidence.

The objective is to obtain a ratio of $D_{combined}/E_{apron}$ as close as possible to one for all the angles and the energies of the incident photon beams considered. Results of $D_{combined}/E_{apron}$ using constants optimized for each dosimeter model will be shown and analysed later.

Table 6. List of the four dosimeters analysed. The detector 1 (low Z filtration) is always case 3A corresponding to the truncated cone, while detector 2 is in turn substituted by all the high Z filtration reported above.

Dosimeter configuration	Low-Z filter (Detector 1)	High-Z filter (Detector 2)
DOSIMETER 1	3A	1B
DOSIMETER 2	3A	2B
DOSIMETER 3	3A	3B
DOSIMETER 4	3A	4B

The curves of the dose responses D_2/K_{air} (*Figure 19*) show the effect of the presence of high Z materials above the detector. In fact, at low energies (20 – 30 keV), for all the configurations, the dose is almost zero due to the high absorption characteristic of these metals. The dose then starts to increase because part the incoming photons with higher energies can pass through the layers of high Z materials and deposit in the detector. The dose continues to increase up to a peak at ~80 keV and decreases sharply at 90 keV due to the k-edge of lead at 88 keV, which corresponds to a maximum of the energy absorption coefficient. A further objective is to increase the dose for energies higher than 88 keV, after the absorption peak. This is possible by introducing a back filter with a k-edge above 88 keV: incident radiation will be backscattered in such filter and will increase the dose in the detector. Additionally, X-ray fluorescence is produced at energies above the k-edge of the material of the filter, which will further increase the dose received by the detector at energies above the k-edge.

The first comparison between different dosimeters will be performed considering always α=1/3.15 and β=1/64, constant for the four dosimeters, so that the changes in the geometry can be seen clearly.

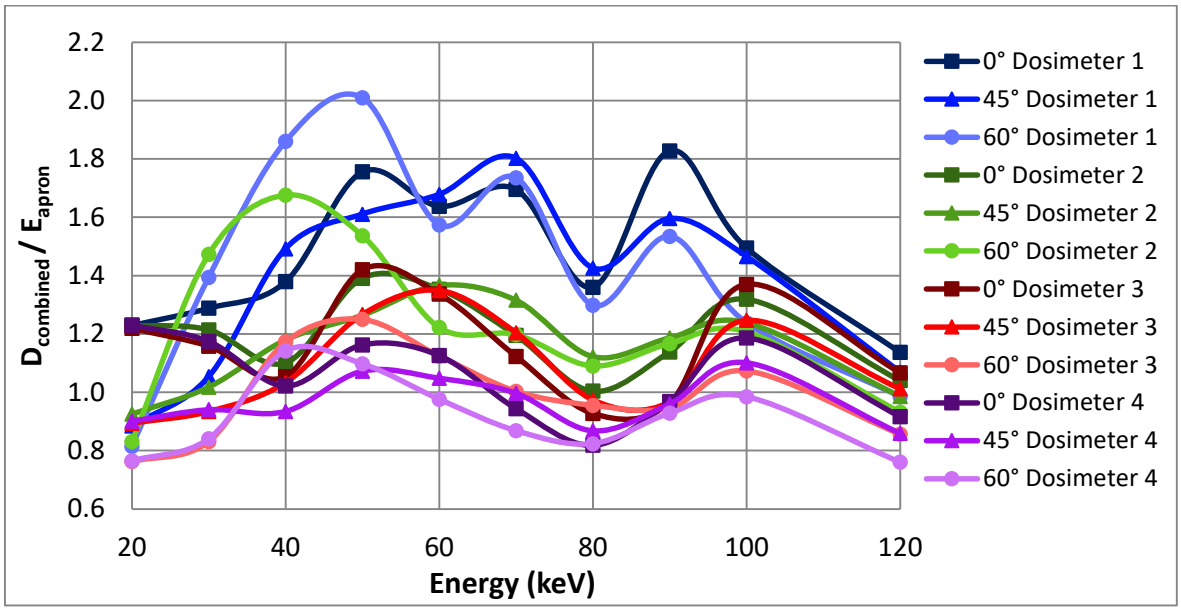

Figure 20. Comparison of the combined dose per effective dose for the four dosimeters considered.

From Figure 20 an immediate comparison among the steps of the first analysis is shown. It can be seen that in dosimeter 1 E_{apron} is strongly overestimated by the dose estimated by the dosimeter ($D_{combined}$) for most photon energies. Then, the dosimeter 2, thanks to the introduction of bismuth above and below, starts to improve the estimation for high energies (from 80 to 120 keV) and reduces also the peak at 90 keV, present in the dosimeter 1. Dosimeter 3 shows the strong improvement of the curves at low energy due to the increase in the thickness of aluminium above the detector (case 3B) while the dosimeter 4 represents a further improvement in the reduction of the overestimation.

All the configurations are now reported considering their own best constants. *Figure 21* will show the results of the combined dose per air kerma, compared to the reference effective dose, as a function of energy of the photon beam.

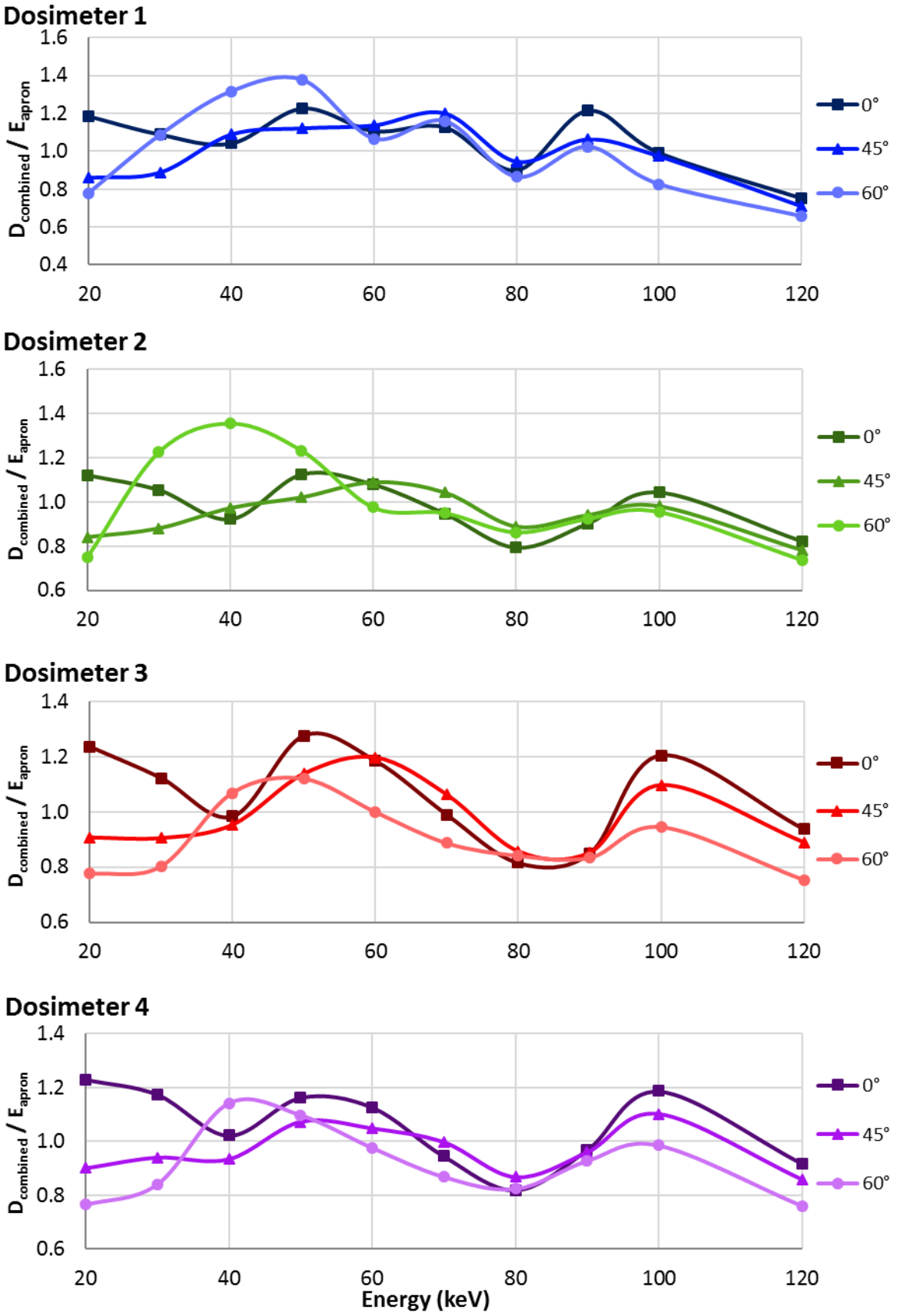

Figure 21. Ratio between the combined dose and the effective dose with lead garments for the four simplified dosimeters.

As can be seen in Figure 21, in the first case (1B) tungsten (Z=74, k-edge at 69.5 keV) is not enough for increasing the dose at high energies because the backscatter is produced in an energy range lower than the necessary one (88 – 120 keV).
This is why in the case 2B, two thin filters of bismuth (Z=83, k-edge at 90.5 keV) are introduced: one above and one below the detector. The filter above the detector reduces the peak at 90 keV, while its presence below helps in increasing the dose at higher energies above 88 keV. In *Figure 19* (case 2B) it can be seen that the introduction of bismuth below the detector almost vanishes the effect of backscattering due to tungsten. Bismuth, in fact, already attenuates incoming photons producing directly backscattering and so preventing them to reach the tungsten layer. This layer is successively removed in case 3B. Moreover, case 3B is also important for the increase of the thickness of aluminium surrounding the detector because it has a positive influence in reducing the overestimation of the combined dose for the radiation coming with the angle of 60°. The choice of aluminium is due to the fact that it is a light material and so it attenuates mainly low energy photons.
Based on the knowledge learnt from the abovementioned cases, the configuration of case 4B has been modelled. In this design the thicknesses of bismuth and lead above have been slightly reduced, while the layer of bismuth below the detector has been halved. This allowed to decrease further the peak of the dose received by the detector (D_2/K_{air}) at 80 keV, and obtain the desired effect of decreasing the peak using a lesser amount of material.
With the last configuration (dosimeter 4, purple curves in Figure 21) the ratio $E_{combined}/E_{apron}$ is always between 0.77 and 1.23 for all photon energies and angles of incidence, *i.e.* the simplified dosimeter 4 can estimate the effective dose with RP garments E_{apron} with a margin of ± 23%. Thus, the over- and the underestimations in case of monoenergetic beams have been reduced from ± 40% in dosimeter 1 to ± 23% in dosimeter 4.

Finally, once obtained a sufficiently accurate result with monoenergetic photon beams, the dose response in case of a more realistic photon beams using spectra have been calculated. As already introduced, the X-ray qualities from the narrow (N) and wide (W) spectra of ISO standard 4037-1 [17] are used for calibration of personal dosimeters, while the RQR spectra from IEC standard 61267 [18] are used to represent the exposure conditions of medical staff in IC and IR. Results of the ratio between the combined dose and the effective dose with lead garments are shown in *Figure 22.*

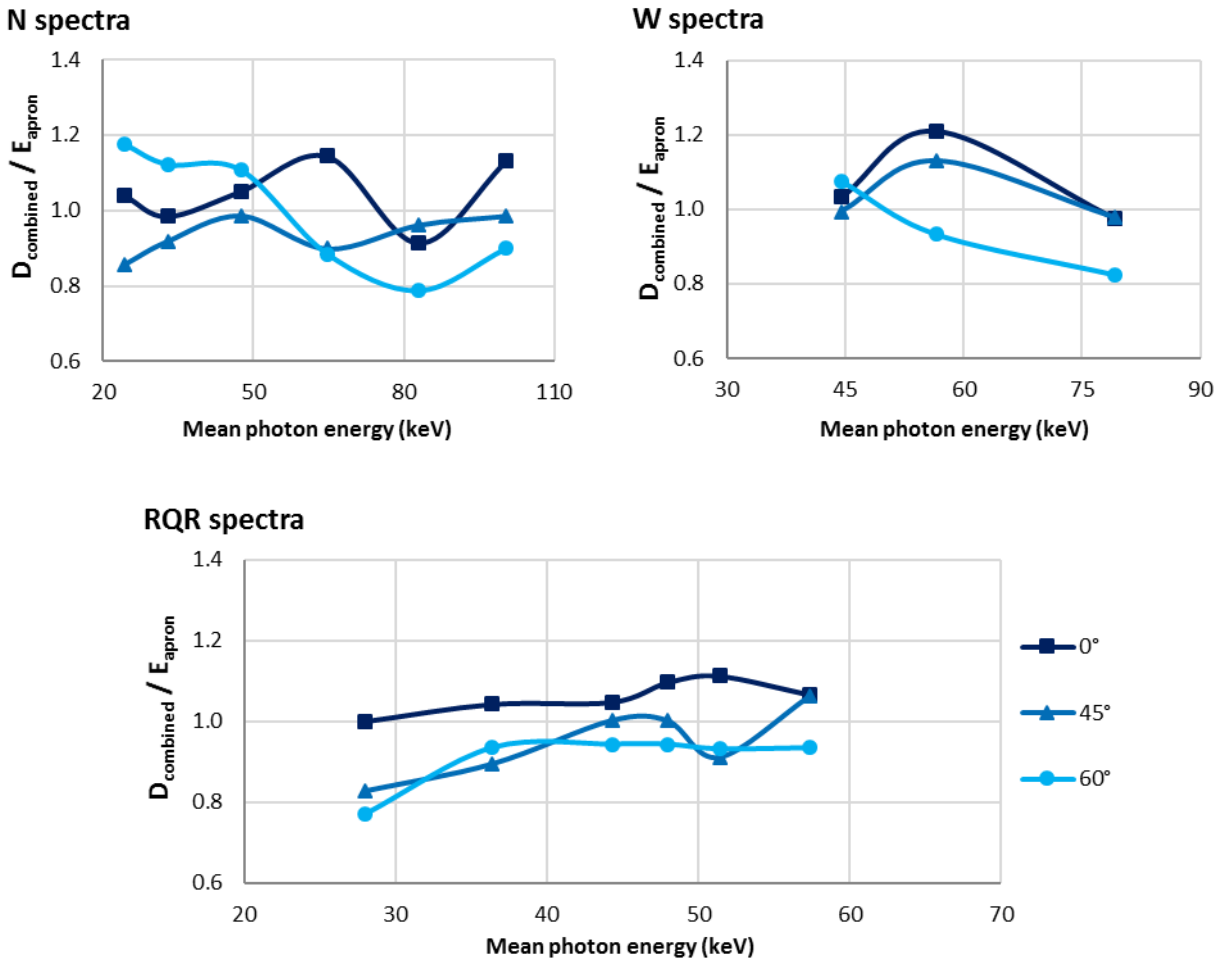

Figure 22. Ratio between the combined dose and the effective dose with RP garments using spectra to reproduce a more realistic photon beams in the case of the simplified dosimeter: N spectra (N30, N40, N60, N80, N100, N120; shown at the top left), W (W60, W80, W110; shown at the top right) and RQR (RQR2, RQR4, RQR6, RQR7, RQR8, RQR9; shown at the bottom).

The results of the spectra are even better with respect to the case of monoenergetic photon beams. For N and W spectra results are in a range of ± 20% of E_{apron} (Figure 22 top), while for RQR spectra, the most interesting result, there is a maximum overestimation of the order of 10% and an underestimation again of 20% as it is visible at the bottom of Figure 22. Another important result is the reduction of the fluctuations of the curves, due to the use of beams with a spectrum of photon energies instead of monoenergetic beams.

3.2 Realistic dosimeter A

The objective of this analysis is to design the new dosimeter with realistic characteristics, taking into account the right geometries and dimensions of the plastic badge and the relative detector with the corresponding filters. This means that the previous two configurations with low and high Z materials, studied separately in the simplified dosimeter, have now to be inserted in the same dosimeter model according to the space available.
First of all, the cylindrical detector is substituted by a parallelepiped of 0.01 cm thickness that constitutes the glass detector used in RPL; then the ABS plastic badge is inserted all around the detector. For the purpose of measuring the two doses with the same detector, detecting volumes have to be chosen. In this first case, the selected detecting volumes have been the one corresponding to the plastic (4) and the copper (2) filters (*Figure 23*). The filters are supposed to be ring parallelepipeds surrounding the detector. At this level of the analysis, the detection volumes have been designed with arbitrary dimensions: 0.4x0.6x0.1 cm^3.

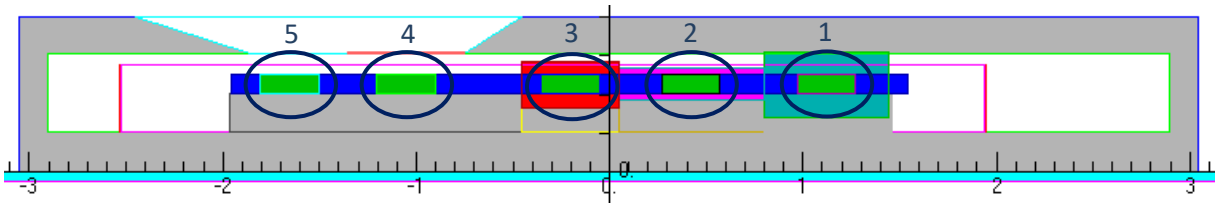

Figure 23. Graphical representation of the structure of the realistic dosimeter A made by a plastic badge and three filters: aluminium, copper and tin.

The characteristics, shapes and dimension of the original filters present in the RPL dosimeter are reported in Table 7.

Table 7. Description of the filters present in the structure of the realistic dosimeter A.

DETECTION POINTS	FILTER	DIMENSIONS (cm)
1	Tin Parallelepiped	$x = 0.65$ $y = 0.94$ $z = 0.34$
2	Copper Parallelepiped	$x = 0.75$ $y = 0.76$ $z = 0.16$
3	Aluminium Parallelepiped	$x = 0.50$ $y = 0.84$ $z = 0.24$
4	No filter	-
5	No filter	-

3.2.1 Low Z filters

As already introduced, now that the dosimeter is one and the detector has five detecting volumes, two of them have to be chosen in order to repeat the same procedure of the simplified dosimeter. In this section the main importance is focused on the high Z filters, thus only two low Z configurations will be reported in the following table.

Table 8. Table of comparison of the cases with low Z materials for the realistic dosimeter A. Front and back filters are summarized with the corresponding shapes and dimensions.

CASE	FRONT FILTERS		BACK FILTERS	
	MATERIAL SHAPE	DIMENSIONS (cm)	MATERIAL SHAPE	DIMENSIONS (cm)
1C	PVC plastic Truncated pyramid	$h = 0.1$ $x_1 = 0.5$ $y_1 = 0.76$ $x_2 = 0.3$ $y_2 = 0.76$	Aluminium Parallelepiped	$x = 0.7$ $y = 0.7$ $z = 0.1$
			Copper Parallelepiped	$x = 1.1$ $y = 0.7$ $z = 0.05$
2C	PVC plastic Truncated pyramid	$h = 0.1$ $x_1 = 0.5$ $y_1 = 0.76$ $x_2 = 0.3$ $y_2 = 76$	Aluminium Parallelepiped	$x = 0.84$ $y = 0.7$ $z = 0.1$

The choice of considering only few configurations related to low Z materials is taken in order to ease the comparison. Case 1C is similar to the low Z filter configuration of the simplified dosimeter but it has been adapted because of the restricted space available, reduced by the design of the plastic badge and the new geometry of the dosimeter, which is now a parallelepiped and no more a cylinder. The new geometry of the detector is also influencing the shape of the PVC. From a truncated cone, the shape passes to a truncated pyramid because in the realistic model there is no more the possibility of surrounding the detector with filters; the truncated pyramid will just be located above it.
This first case (1C) will be used for combining the dose of all the future cases of high Z materials while case 2C will be used only for the last one.

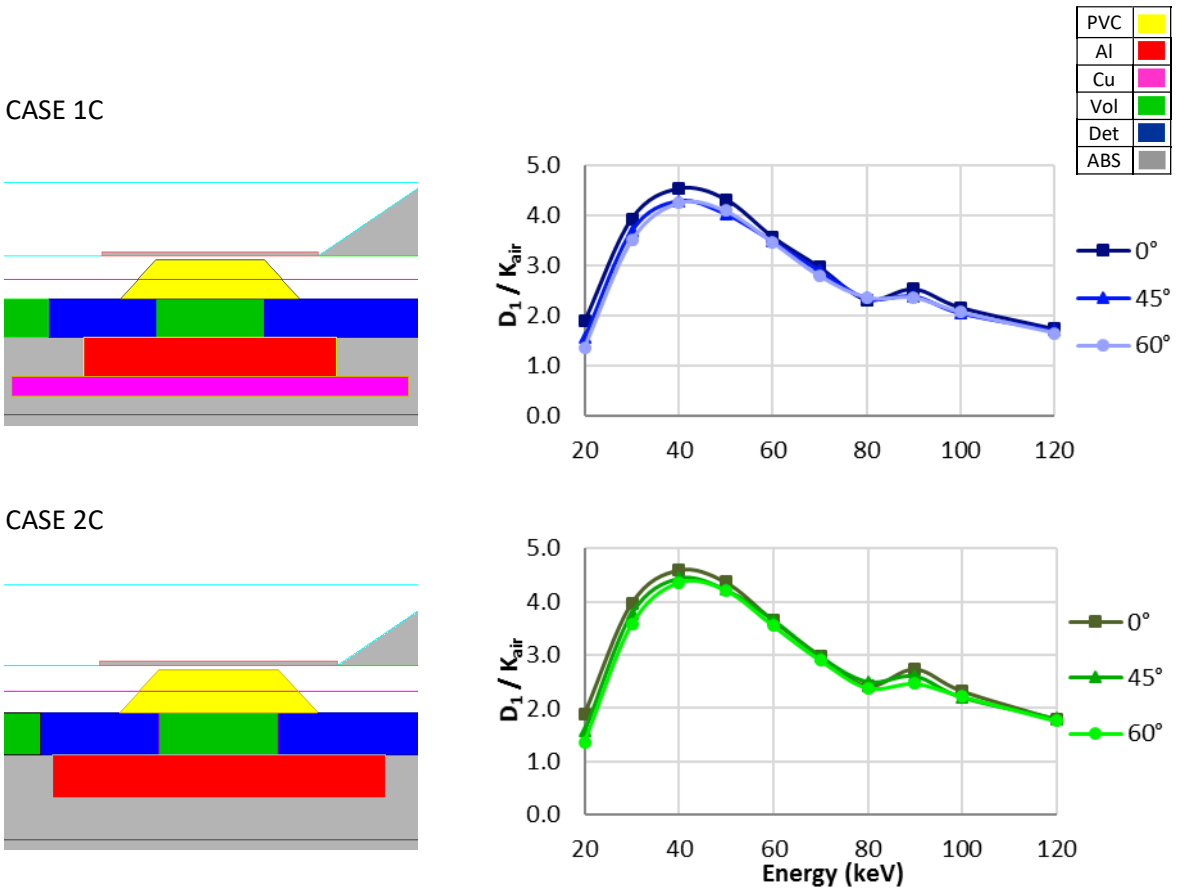

Figure 24. Low Z filter configurations and corresponding response of the detector volume 1 of therealistic dosimeter A in terms of dose per air kerma.

Cases 1C and 2C differ from one another only in the presence or absence of copper below the detector. Copper should give an influence in reducing the backscatter radiation (peak at ~90 keV) caused by the presence of lead but in this new design it can be avoided because the effect is almost negligible. In fact the only distinction between the two cases, even if not so noticeable, regards the peak at ~90 keV; as expected there is a slight increase of the dose response in that peak when the layer of copper is removed (case 2C in *Figure 24*).

The strong energy dependence of the dosimeter is again evident in this part of the analysis, exactly like the cases of the simplified dosimeter.

3.2.2 High Z filters

The following table summarizes the cases selected to present all the steps of the optimization of the high Z filtration.

Table 9. Table of comparison of the cases with high Z materials for the realistic dosimeter A. Front and back filters are summarized with the corresponding shapes and dimensions.

CASE	FRONT FILTERS		BACK FILTERS	
	MATERIAL SHAPE	DIMENSIONS (cm)	MATERIAL SHAPE	DIMENSIONS (cm)
1D	Lead Parallelepiped	$x = 0.65$ $y = 0.76$ $z = 0.025$	Tin Parallelepiped	$x = 0.75$ $y = 0.76$ $z = 0.06$
	Bismuth Parallelepiped	$x = 0.65$ $y = 0.76$ $z = 0.025$	Tungsten Parallelepiped	$x = 0.75$ $y = 0.76$ $z = 0.02$
2D	Lead Parallelepiped	$x = 0.65$ $y = 0.76$ $z = 0.03$	Tin Parallelepiped	$x = 0.45$ $y = 0.76$ $z = 0.02$
	Bismuth Parallelepiped	$x = 0.65$ $y = 0.76$ $z = 0.03$	Tungsten Parallelepiped	$x = 0.75$ $y = 0.76$ $z = 0.03$
	Copper Parallelepiped + Air gap Parallelepiped	$x_1 = 0.75$ $y_1 = 0.76$ $z_1 = 0.03$ $x_2 = 0.31$ $y_2 = 0.40$ $z_2 = 0.03$	-	-

Table 9 (continuation). Table of comparison of the cases with high Z materials for the realistic dosimeter A. Front and back filters are summarized with the corresponding shapes and dimensions.

CASE	FRONT FILTERS		BACK FILTERS	
	MATERIAL SHAPE	DIMENSIONS (cm)	MATERIAL SHAPE	DIMENSIONS (cm)
3D	Lead Parallelepiped	$x = 0.65$ $y = 0.76$ $z = 0.03$	Tin Parallelepiped	$x = 0.35$ $y = 0.76$ $z = 0.03$
	Bismuth Parallelepiped	$x = 0.65$ $y = 0.76$ $z = 0.03$	Tungsten Parallelepiped	$x = 0.75$ $y = 0.76$ $z = 0.04$
	Copper Parallelepiped + Air gap Parallelepiped	$x_1 = 0.75$ $y_1 = 0.76$ $z_1 = 0.04$ $x_2 = 0.31$ $y_2 = 0.40$ $z_2 = 0.04$	-	-
4D	Lead Parallelepiped	$x = 0.65$ $y = 0.76$ $z = 0.04$	Tin Parallelepiped	$x = 0.45$ $y = 0.76$ $z = 0.03$
	Bismuth Parallelepiped	$x = 0.65$ $y = 0.76$ $z = 0.02$	Tungsten Parallelepiped	$x = 0.75$ $y = 0.76$ $z = 0.04$
	Copper Parallelepiped + Air gap Parallelepiped	$x_1 = 0.75$ $y_1 = 0.76$ $z_1 = 0.04$ $x_2 = 0.41$ $y_2 = 0.40$ $z_2 = 0.04$	-	-
5D	Lead (1) Parallelepiped	$x = 0.30$ $y = 0.76$ $z = 0.02$	Tin Parallelepiped	$x = 0.65$ $y = 0.76$ $z = 0.08$
	Lead (2) Parallelepiped	$x = 0.69$ $y = 0.76$ $z = 0.03$	Tungsten (1) Parallelepiped	$x = 0.75$ $y = 0.76$ $z = 0.08$
	Bismuth Parallelepiped	$x = 0.69$ $y = 0.76$ $z = 0.02$	Tungsten (2) Parallelepiped	$x = 0.75$ $y = 0.76$ $z = 0.06$
	Copper Parallelepiped + Air gap Parallelepiped	$x_1 = 0.75$ $y_1 = 0.76$ $z_1 = 0.03$ $x_2 = 0.31$ $y_2 = 0.40$ $z_2 = 0.03$	-	-

Table 9 (continuation). Table of comparison of the cases with high Z materials for the realistic dosimeter A. Front and back filters are summarized with the corresponding shapes and dimensions.

CASE	FRONT FILTERS		BACK FILTERS	
	MATERIAL SHAPE	DIMENSIONS (cm)	MATERIAL SHAPE	DIMENSIONS (cm)
6D	Lead (1) Parallelepiped	$x = 0.30$ $y = 0.76$ $z = 0.02$	Tin Parallelepiped	$x = 0.65$ $y = 0.76$ $z = 0.10$
	Lead (2) Parallelepiped	$x = 0.69$ $y = 0.76$ $z = 0.03$	Tungsten (1) Parallelepiped	$x = 0.75$ $y = 0.76$ $z = 0.08$
	Bismuth Parallelepiped	$x = 0.65$ $y = 0.76$ $z = 0.02$	Tungsten (2) Parallelepiped	$x = 0.75$ $y = 0.76$ $z = 0.06$
	Copper Parallelepiped + Air gap Parallelepiped	$x_1 = 1.05$ $y_1 = 0.76$ $z_1 = 0.03$ $x_2 = 0.31$ $y_2 = 0.40$ $z_2 = 0.03$	-	-

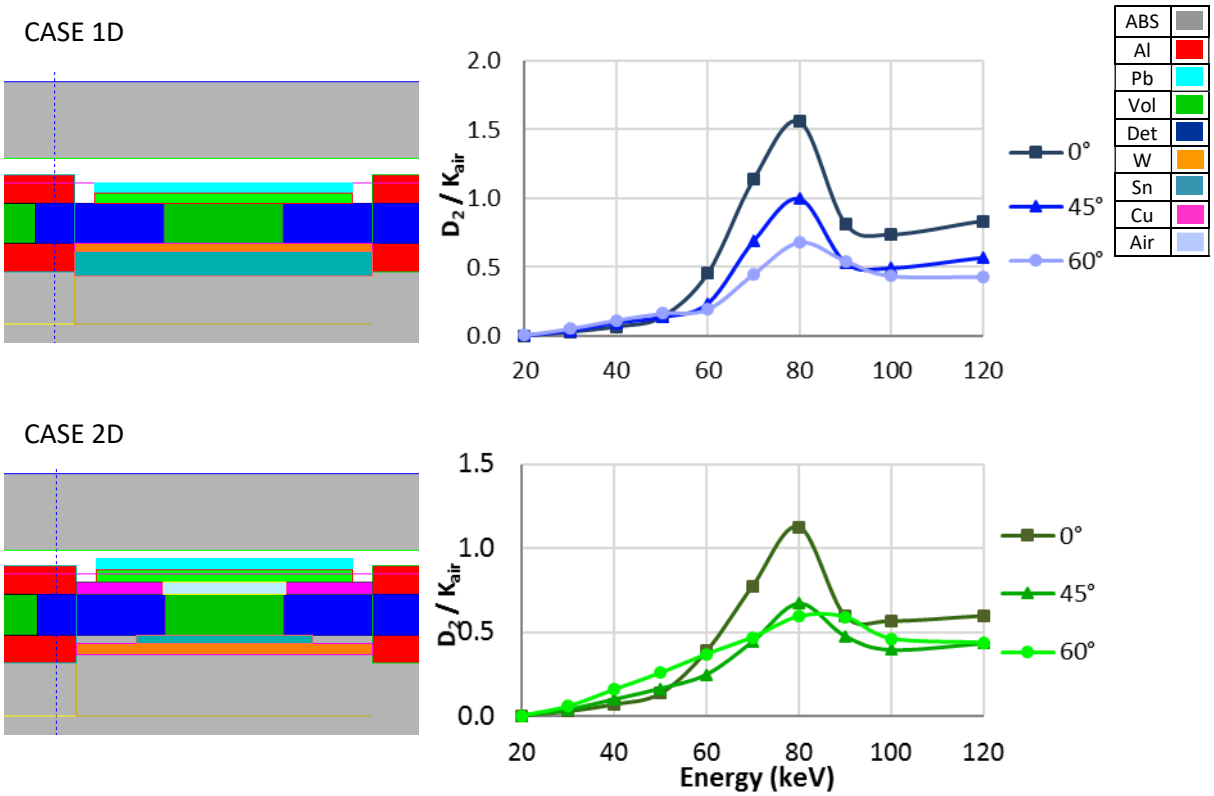

Figure 25. High Z filter configurations and corresponding response of the realistic dosimeter A in terms of dose per air kerma.

CASE 3D

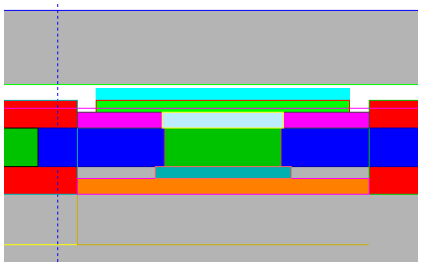

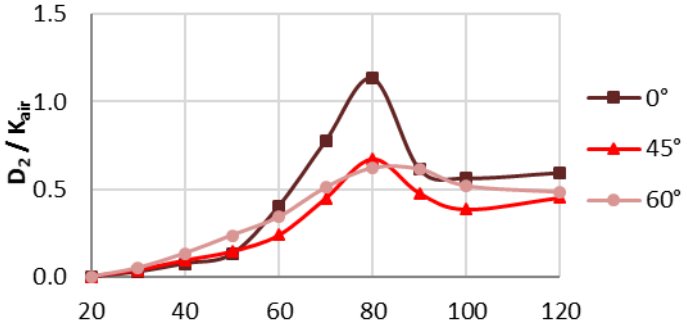

CASE 4D

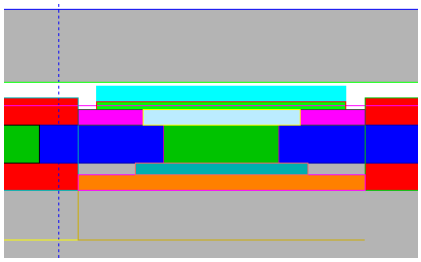

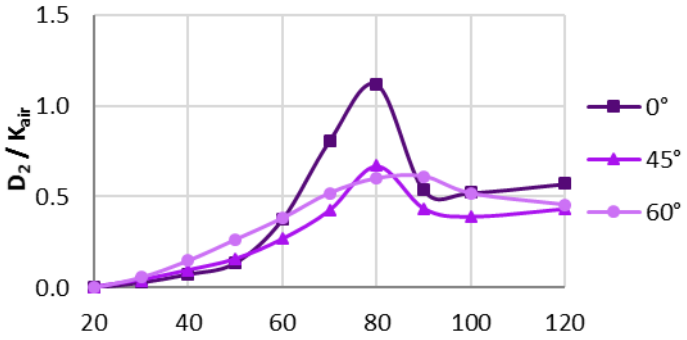

CASE 5D

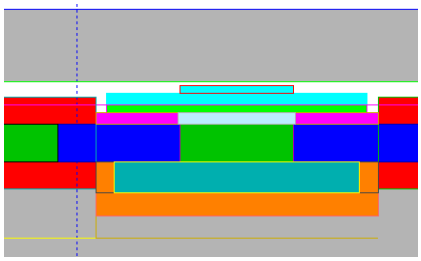

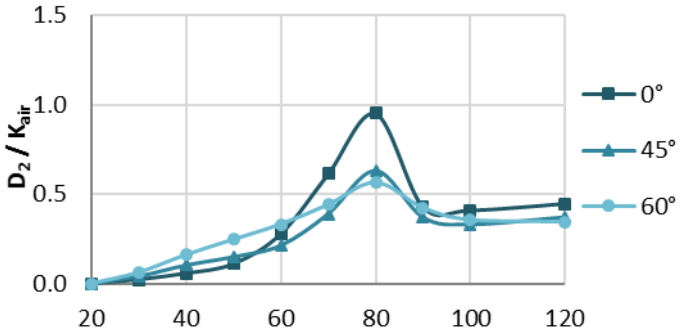

CASE 6D

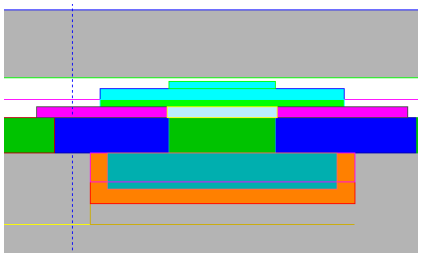

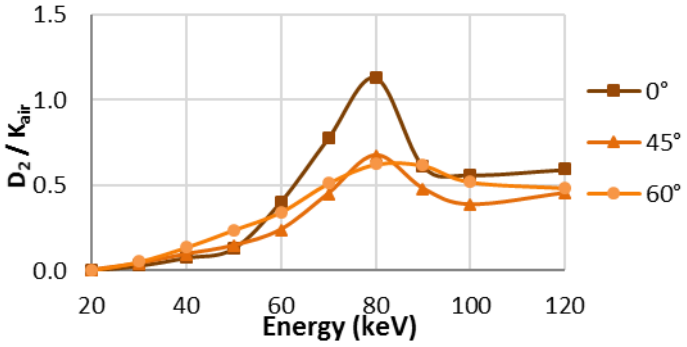

Figure 25 (continuation). High Z filter configurations and corresponding response of the realistic dosimeter A in terms of dose per air kerma.

All the combinations to obtain the realistic dosimeter A are reported in *Table 10*, below.

Table 10. List of the six dosimeter analysed. The detector 1 (low Z filtration) is case 1C for all the five detectors 2, while case 2C is used to combine the dose of the last high Z geometry.

Dosimeter configuration	Low-Z filter (Detector 1)	High-Z filter (Detector 2)
DOSIMETER 1	1C	1D
DOSIMETER 2	1C	2D
DOSIMETER 3	1C	3D
DOSIMETER 4	1C	4D
DOSIMETER 5	1C	5D
DOSIMETER 6	2C	6D

In all the steps, as in the simplified dosimeter, the objective is to reduce the peak of the dose at 80 keV. In the first five cases the pre-existing aluminium filter has been kept, the copper filter has been removed, while the tin one has been substituted by another aluminium filter because its high Z it was influencing significantly in terms of attenuation the beam coming with an angle of incidence of 60°. The choice of substituting, from case 1D to 5D, with aluminium has been made for matters of symmetry and also because aluminium, having a lower Z, has less impact. In the realistic dosimeter bismuth below the detector is not useful anymore, but some backscattering is needed between 40 and 70 keV, which explains the introduction of materials like tin (Z=50, k-edge at 29 keV) and tungsten (Z=74, k-edge at 70 keV). The design above the detector is instead kept very similar to the one that characterized the simplified dosimeter, made by lead bismuth, but with the introduction of a liner of copper instead of titanium.

Figure 26 shows all the graphs of the ratio between the combined dose and the effective dose with lead garments evaluated for monoenergetic photon beams, for the case of the realistic dosimeter A.

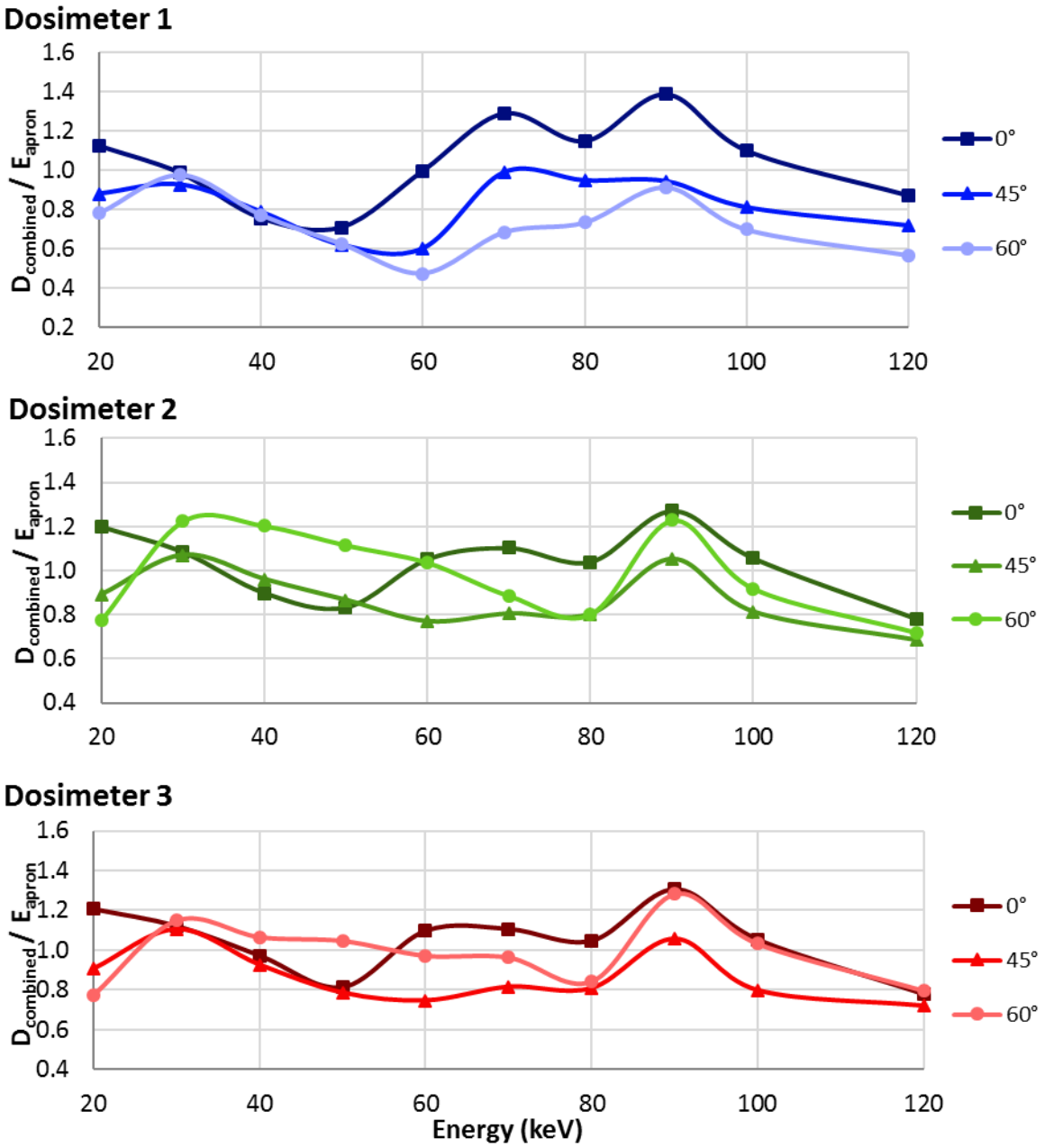

Figure 26. Ratio between the combined dose and the effective dose with lead garments for the six dosimeters.

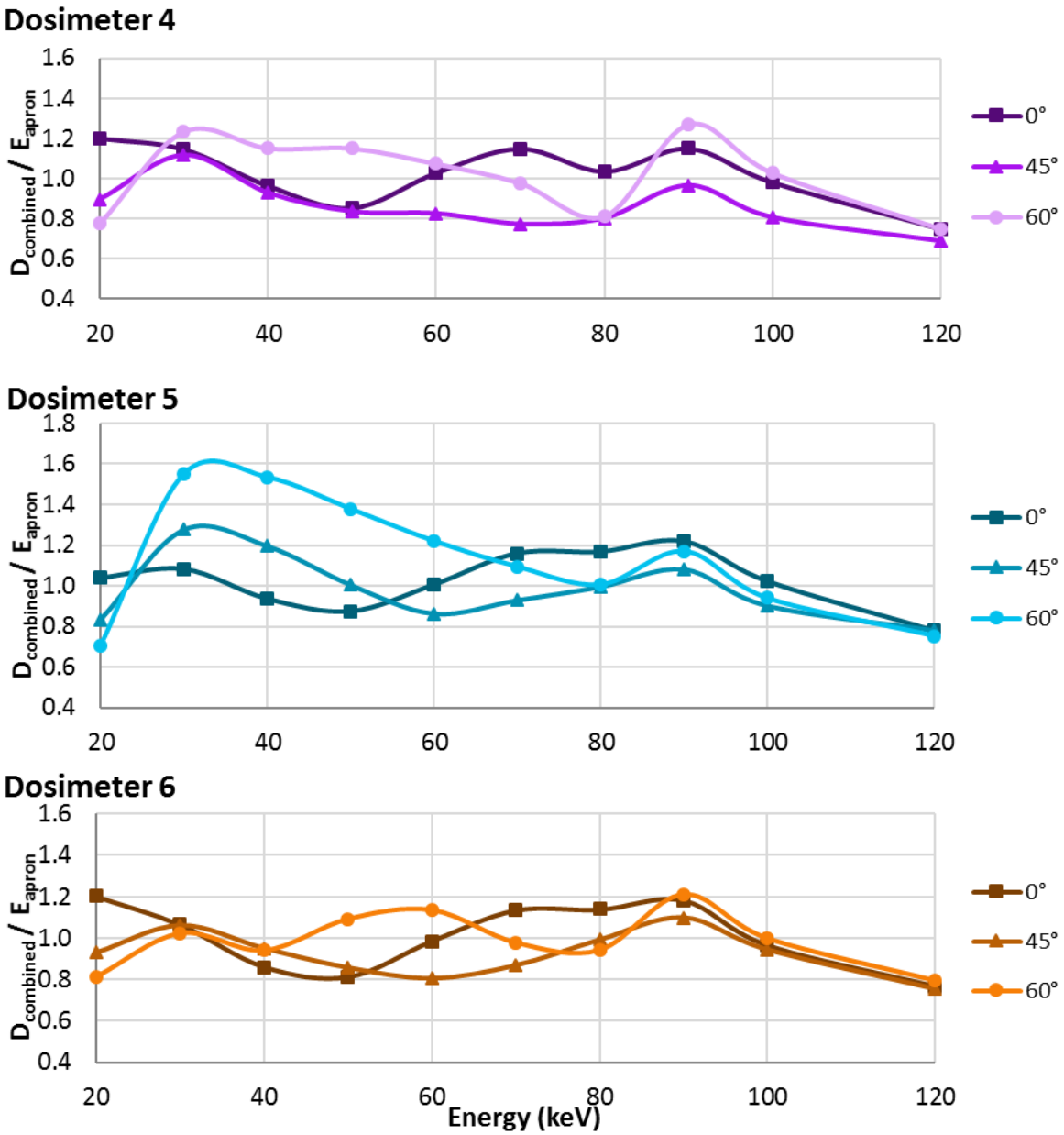

Figure 26 (continuation). Ratio between the combined dose and the effective dose with lead garments for the six dosimeters.

At the beginning a sort of reproduction of the filters selected for the simplified geometry has been performed (dosimeter 1), despite the difficult task of fitting them in the plastic badge, which has fixed dimensions. The outcomes of the simulations did not bring acceptable results (*Figure 26*, blue curves), so a new configuration has been projected using simpler geometries of filters (parallelepipeds). Bismuth and lead over the detecting volume representing the high Z configuration are still necessary to attenuate high energy photons.

The expectation of increasing the dose in the dosimeter 1 in that range of energy between 40 and 70 keV, introducing a liner of tin and another of tungsten, is actually satisfied only for energies higher than 70 keV. This can be explained by the position of the filters; the tungsten, inserted directly below the detector, shields photons and creates backscattering preventing them to arrive to the tin, which is located below. In order to have an effect in that range of energies, photons should pass through tungsten, and the ones backscattered in the tin should cross the tungsten filter again, to reach the detecting volume. The effect of tin in this position is almost useless, in fact from *Figure 26* it is not possible to see an increase of the dose. The constants in the case of dosimeter 1 are $\alpha=1/3$ and $\beta=1/100$.

The purpose of the next simulation (dosimeter 2) is to overcome the problem of the dosimeter 1 inverting the filters, which means putting tin in direct contact with the detector, followed by tungsten. The tin filter has also been reduced in dimension with respect to the tungsten one, in this way the 60° curve should feel more the influence of tungsten.

The curve corresponding to 0° shows a strong overestimation at high energies, which means that attenuation of the front filters is not enough; for this reason, the amount of lead above has been increased. Moreover, a new filter is introduced on top of the detector: a copper parallelepiped with a layer of air just above the detecting volume. The objective of the air above is to avoid scattering that can be present due to the contact of bismuth with the detector, that would result in a further increase of the dose, which is not needed.

Many improvements can be noticed, but still the peak at 90 keV is high and the doses corresponding to the beam coming with the angle of 60° should be decreased for low energies. The constants in the case of the dosimeter 2 are $\alpha=1/2.4$ and $\beta=1/120$.

The thickness of copper above the detecting volume has been increased to give a stronger contribution in shielding radiation coming with the angle of $60°$ at low energies. Also the amount of tin and tungsten below the detector has been increased to improve their contribution. The peak corresponding to 90 keV hasn't been flattened but contrarily it is a little bit higher than in the previous case, because the increase of copper pushes a little bit further from the detector bismuth and lead filters, reducing their effectiveness.

The reduction of the *x* dimension of tin is instead noticed by the underestimation in the range of 50 - 60 keV for the curve of $45°$ and so it does not contribute positively to the analysis. The constants in the case of dosimeter 3 are $\alpha=1/2.4$ and $\beta=1/120$.

Due to the peak at 90 keV, in order to keep the presence of more copper just above the detector, a thicker layer of lead is substituted to the previous one. The dimension on the *x* direction of the tin filter has been restored with the aim of giving a higher contribution of backscattering in that area for the angle of 45°.

In this configuration also the air gap above the detector is increased but the result is only a smaller contribution of the copper filter. The geometry tested is still not optimal for the angle of 45° because of the strong underestimation and for the angle of 60° for the strong fluctuation of the values at high energy. The constants in the case of dosimeter 4 are $\alpha=1/2.4$ and $\beta=1/120$.

The following step has been to increase bismuth and lead filters in the *x* and *y* directions (area of the filter) with the aim of attenuating better the curve for 60°, bringing back the thicknesses to the previous values but adding a smaller layer on top, to raise the shielding contribution for 0°. Also the thicknesses of copper and air have been reduced up to the initial value because the increase did not produce a significant effect. Moreover, tin and tungsten filters have been increased in thickness and an amount of tungsten has been added surrounding the tin filter.

The result of dosimeter 5 is considerably better for high energy photon beams; the peaks are now less sharp and the curves have a similar behaviour. The worst part is now an overestimation of the curves of 45° and 60° in the low energy region; this might be due to the increase of the thickness, x and y directions of the bismuth and lead filters above the detecting volume that results in a higher coverage of the copper filter, which becomes ineffective. The constants in the case of dosimeter 5 are $\alpha=1/1.8$ and $\beta=1/190$.

The last geometry has been optimized through the elimination of the aluminium filters, and the increase of the quantity of copper above the detector in terms of area, resulting in a really strong reduction of the overestimation of the curve of 60° at low energies.

The tin present below has been increased, but this has a negligible effect in the final result.

With respect to the previous cases, the low Z design has been slightly modified, eliminating the copper filter below the detecting volume. The choice does not influence considerably the results also because there is a quite thick amount of aluminium that reduces the influence of copper. The combined dose in this first case of realistic geometry with big detecting volumes is in a range of ± 20% of underestimation and overestimation with respect to the reference effective dose with lead garments E_{apron}. The constants in case of the dosimeter 6 are $\alpha=1/1.8$ and $\beta=1/160$.

Considering the design of the dosimeter 6, the simulations have been performed again taking into account radiation qualities.

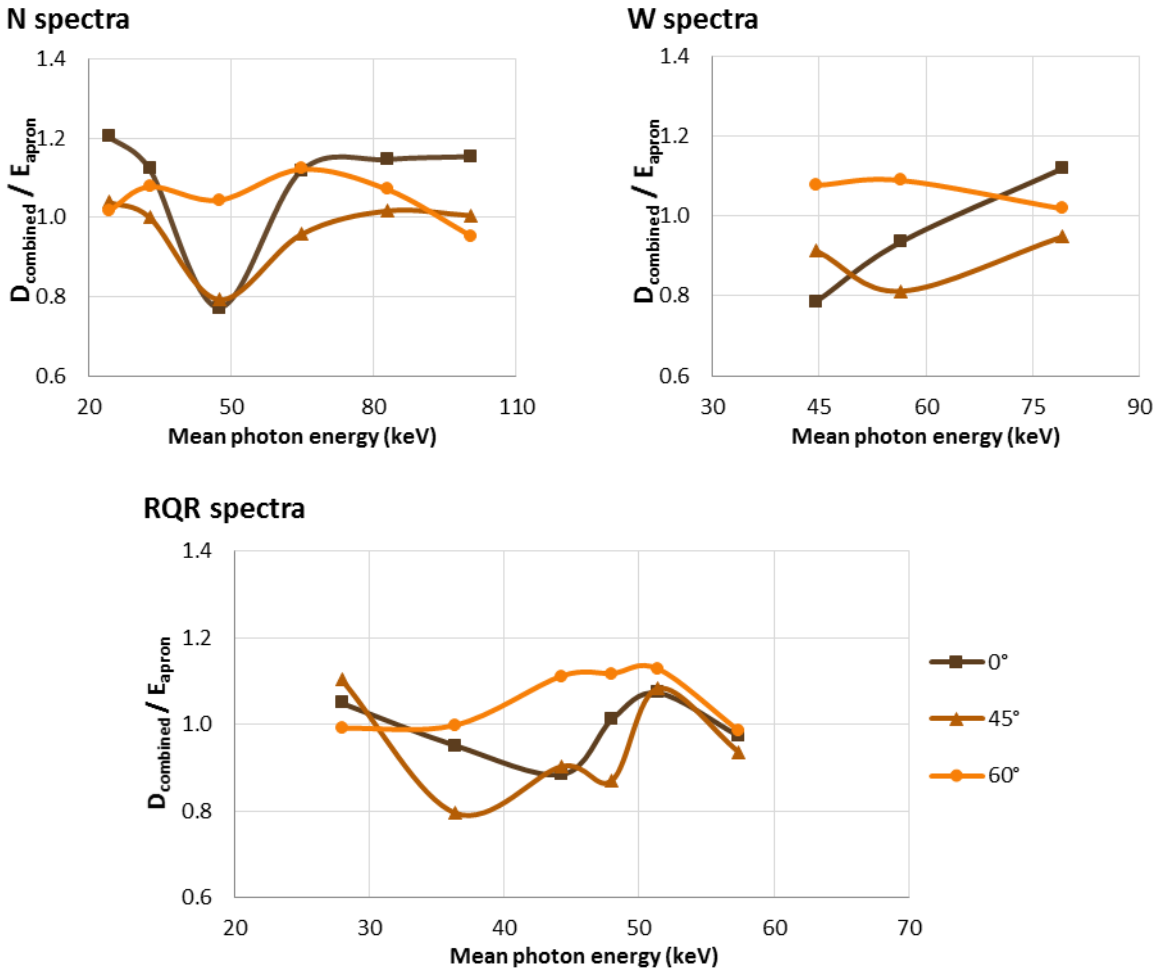

Figure 27. Ratio between the combined dose and the effective dose with RP garments using spectra to reproduce a more realistic exposure in the case of the realistic dosimeter A: N spectra (N30, N40, N60, N80, N100, N120; shown at the top left), W (W60, W80, W110; shown at the top right) and RQR (RQR2, RQR4, RQR6, RQR7, RQR8, RQR9; shown at the bottom).

At the bottom of *Figure 27*, the curves of RQR spectra show a maximum overestimation of 15% and a maximum underestimation of 20%. The strong decrease at around 40 – 50 keV with N spectra is due to the fact that they are narrower and more similar to the monoenergetic beams with respect to W and RQR spectra, in which the peak is less marked.

3.3 Realistic dosimeter B

A further improvement of the geometry has been carried out changing the dimensions of the detecting volumes, which now are 0.17x0.3x0.05 cm^3 (compared to 0.4x0.6x0.1 cm^3 detecting volumes of the previous realistic dosimeter). The plastic badge and the filters position and dimension are the same of the one analysed in the realistic dosimeter A. Also the detection volumes selected to perform the evaluation of the effective dose are the same as before to ease the comparison of the results.

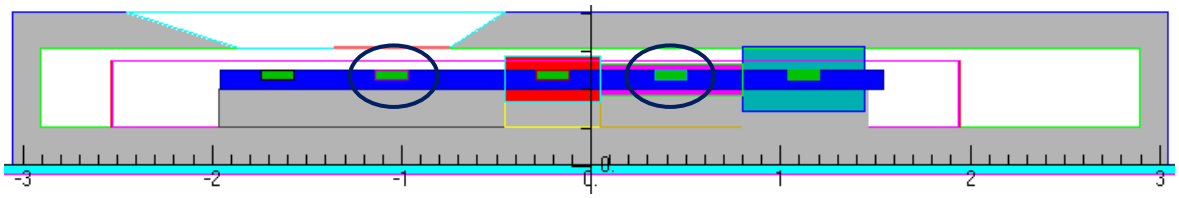

Figure 28. Graphical representation of the structure of the realistic dosimeter B. The circles represent the two detecting volumes selected for the insertion of the filtration.

3.3.1 Low Z filters

A particular attention is focused on this section, which presents some among the low Z configurations used in the simulations. The need of improving the dose response in case of low Z filtration is due to the low values to the constant β used, up to now, in the realistic dosimeter A. Having a low constant means that the contribution of the low Z filtration is reduced a lot thus it becomes almost useless, which allows to understand that the dose received by the detector is actually too high; for this reason, higher Z materials with respect to PVC are introduced to increase the filtration (*Table 11*).

Table 11. Table of comparison of the cases with low Z materials for the realistic dosimeter B. Front and back filters are summarized with the corresponding shapes and dimensions.

CASE	FRONT FILTERS		BACK FILTERS	
	MATERIAL SHAPE	DIMENSIONS (cm)	MATERIAL SHAPE	DIMENSIONS (cm)
1	PVC plastic Truncated pyramid	$h = 0.1$ $x_1 = 0.5$ $y_1 = 0.76$ $x_2 = 0.3$ $y_2 = 0.76$	Aluminium Parallelepiped	$x = 0.84$ $y = 0.7$ $z = 0.1$
2	Aluminium Truncated pyramid	$h = 0.1$ $x_1 = 0.5$ $y_1 = 0.76$ $x_2 = 0.3$ $y_2 = 0.76$	-	-

Table 11 (continuation). Table of comparison of the cases with low Z materials for the realistic dosimeter B. Front and back filters are summarized with the corresponding shapes and dimensions.

CASE	FRONT FILTERS		BACK FILTERS	
	MATERIAL SHAPE	DIMENSIONS (cm)	MATERIAL SHAPE	DIMENSIONS (cm)
3	Titanium Truncated pyramid	$h = 0.1$ $x_1 = 0.5$ $y_1 = 0.76$ $x_2 = 0.3$ $y_2 = 0.76$	-	-
4	Titanium Parallelepiped	$x = 0.50$ $y = 0.76$ $z = 0.03$	-	-
	Aluminium Parallelepiped	$x = 0.50$ $y = 0.76$ $z = 0.03$	-	-
5	Titanium Truncated pyramid	$h = 0.015$ $x_1 = 0.26$ $y_1 = 0.76$ $x_2 = 0.17$ $y_2 = 0.76$	-	-
	Aluminium Truncated pyramid	$h = 0.11$ $x_1 = 0.8$ $y_1 = 0.76$ $x_2 = 0.4$ $y_2 = 0.76$	-	-
6	Titanium Parallelepiped	$x = 0.18$ $y = 0.76$ $z = 0.02$	-	-
	Aluminium Truncated pyramid	$h = 0.11$ $x_1 = 0.8$ $y_1 = 0.76$ $x_2 = 0.4$ $y_2 = 0.76$	-	-
7	Titanium Parallelepiped	$x = 0.18$ $y = 0.76$ $z = 0.02$	-	-
	Aluminium Truncated pyramid	$h = 0.11$ $x_1 = 0.7$ $y_1 = 0.76$ $x_2 = 0.3$ $y_2 = 0.76$	-	-

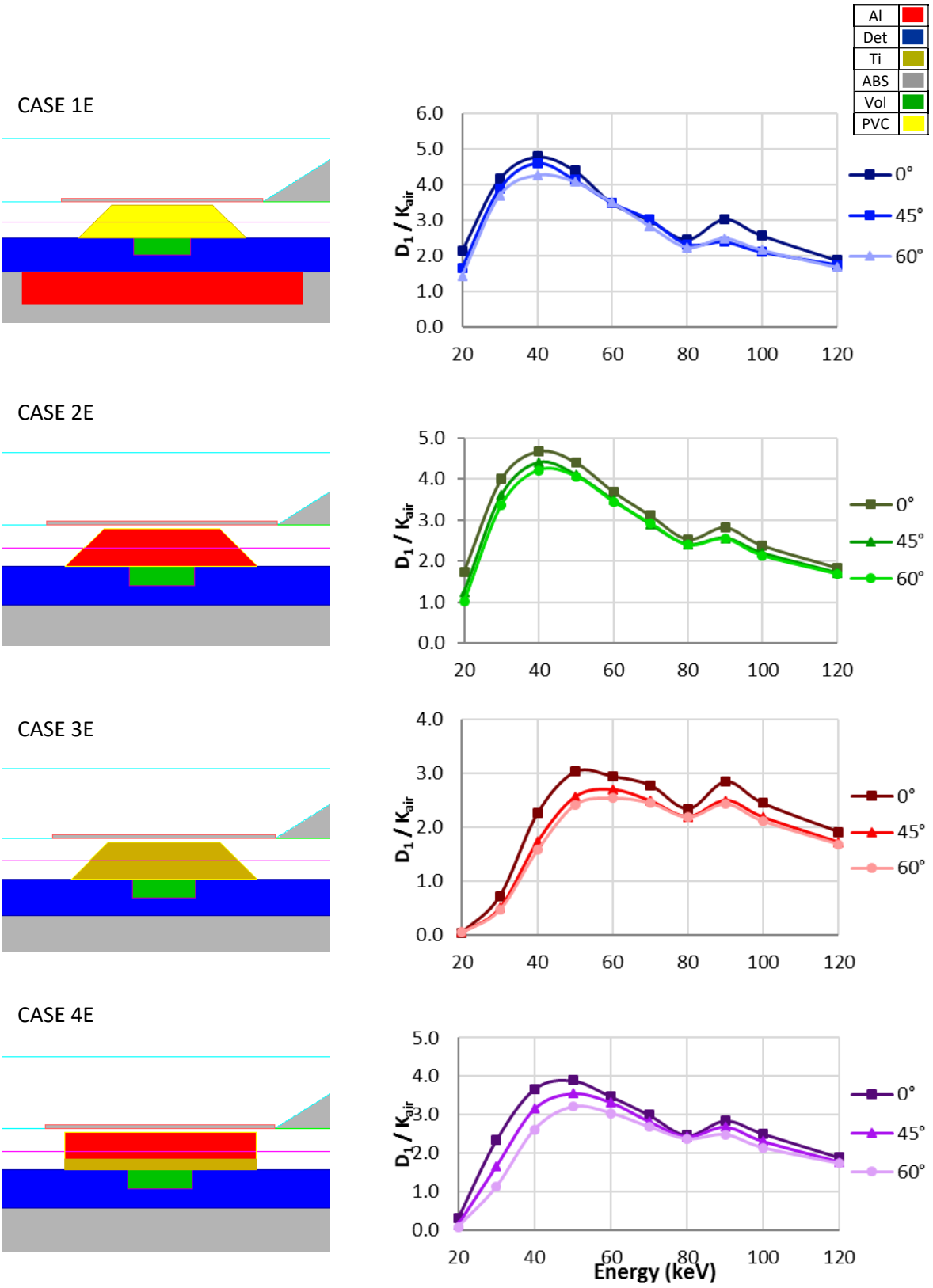

Figure 29. Low Z filter configurations and corresponding response of the realistic dosimeter B in terms of dose per air kerma.

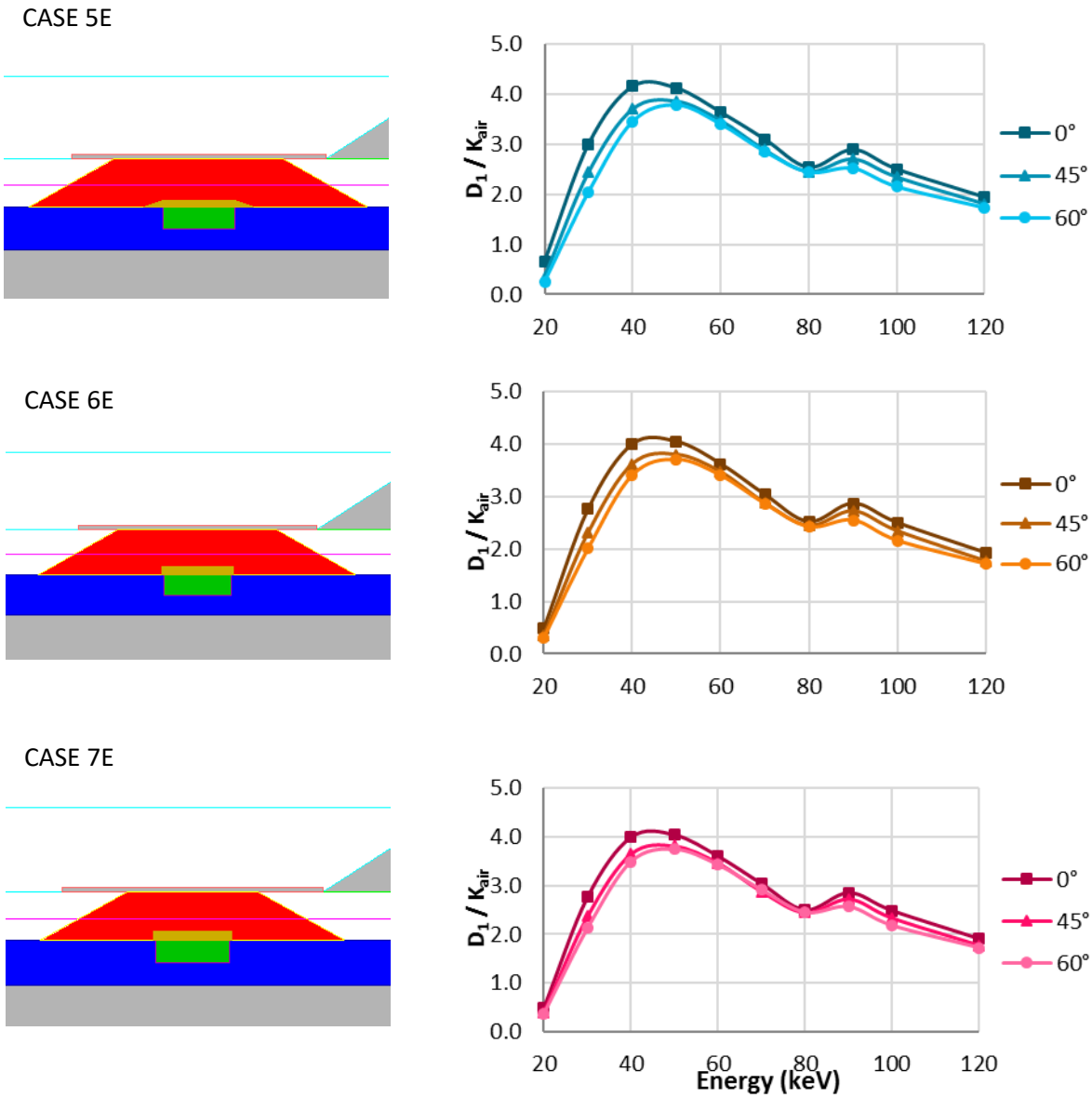

Figure 29 (continuation). Low Z filter configurations and corresponding response of the realistic dosimeter B in terms of dose per air kerma.

The initial PVC filter (case 1E) has been substituted first of all by aluminium (Z=13) in case 2E, then by titanium (Z=22) in case 3E, without modifying the truncated pyramid shape, which is useful for the angular dependence. The design with aluminium was not shielding enough the incoming radiation while the one made by titanium is instead underestimating too much the dose, in particular at 20 keV. In order to overcome this issue, a combination of these two filters has been chosen (case 4E). The case of two layers made by parallelepiped still pointed out a strong shielding due to titanium, therefore the following step has been to introduce a small layer, first a small truncated pyramid (case 5E) and then a parallelepiped (cases 6E), inside a bigger filter made of aluminium. The final design has been the best compromise among the dimensions and shapes tested, always trying to simplify the geometries of the various filters (case 7E), as presented in *Figure 29*.

3.3.2 High Z filters

The following table (*Table 12*) summarizes the cases with high Z filtration. It is possible to notice that all of them are already characterized by the absence of pre-existent filters around.

Table 12. Table of comparison of the cases with high Z materials for the realistic dosimeter B. Front and back filters are summarized with the corresponding shapes and dimensions.

CASE	FRONT FILTERS		BACK FILTERS	
	FRONT FILTERS	DIMENSIONS (cm)	BACK FILTERS	DIMENSIONS (cm)
1F	Lead (1) Parallelepiped	$x = 0.30$ $y = 0.76$ $z = 0.02$	Tin Parallelepiped	$x = 0.65$ $y = 0.76$ $z = 0.08$
	Lead (2) Parallelepiped	$x = 0.69$ $y = 0.76$ $z = 0.03$	Tungsten Parallelepiped	$x = 0.75$ $y = 0.76$ $z = 0.14$
	Bismuth Parallelepiped	$x = 0.69$ $y = 0.76$ $z = 0.02$	-	-
	Copper Parallelepiped + Air gap Parallelepiped	$x_1 = 1.05$ $y_1 = 0.76$ $z_1 = 0.03$ $x_2 = 0.31$ $y_2 = 0.40$ $z_2 = 0.03$	-	-
2F	Lead (1) Parallelepiped	$x = 0.17$ $y = 0.76$ $z = 0.02$	Tin Parallelepiped	$x = 0.45$ $y = 0.76$ $z = 0.05$
	Lead (2) Parallelepiped	$x = 0.55$ $y = 0.76$ $z = 0.03$	Tungsten Parallelepiped	$x = 0.55$ $y = 0.76$ $z = 0.10$
	Bismuth Parallelepiped	$x = 0.55$ $y = 0.76$ $z = 0.02$	-	-
	Copper Parallelepiped + Air gap Parallelepiped	$x_1 = 0.77$ $y_1 = 0.76$ $z_1 = 0.03$ $x_2 = 0.18$ $y_2 = 0.40$ $z_2 = 0.03$	-	-

Table 12 (continuation). Table of comparison of the cases with high Z materials for the realistic dosimeter B. Front and back filters are summarized with the corresponding shapes and dimensions.

CASE	FRONT FILTERS		BACK FILTERS	
	FRONT FILTERS	DIMENSIONS (cm)	BACK FILTERS	DIMENSIONS (cm)
3F	Lead (1) Parallelepiped	$x = 0.17$ $y = 0.76$ $z = 0.02$	Tin Parallelepiped	$x = 0.45$ $y = 0.76$ $z = 0.03$
	Lead (2) Parallelepiped	$x = 0.55$ $y = 0.76$ $z = 0.03$	Tungsten Parallelepiped	$x = 0.55$ $y = 0.76$ $z = 0.07$
	Bismuth Parallelepiped	$x = 0.55$ $y = 0.76$ $z = 0.02$	-	-
	Copper Parallelepiped + Air gap Parallelepiped	$x_1 = 0.79$ $y_1 = 0.76$ $z_1 = 0.03$ $x_2 = 0.18$ $y_2 = 0.40$ $z_2 = 0.03$	-	-
4F	Lead (1) Parallelepiped	$x = 0.17$ $y = 0.76$ $z = 0.02$	Tin Parallelepiped	$x = 0.45$ $y = 0.76$ $z = 0.02$
	Lead (2) Parallelepiped	$x = 0.55$ $y = 0.76$ $z = 0.03$	Tungsten Parallelepiped	$x = 0.55$ $y = 0.76$ $z = 0.05$
	Bismuth Parallelepiped	$x = 0.55$ $y = 0.76$ $z = 0.02$	-	-
	Copper Parallelepiped + Air gap Parallelepiped	$x_1 = 0.81$ $y_1 = 0.76$ $z_1 = 0.04$ $x_2 = 0.15$ $y_2 = 0.40$ $z_2 = 0.04$	-	-

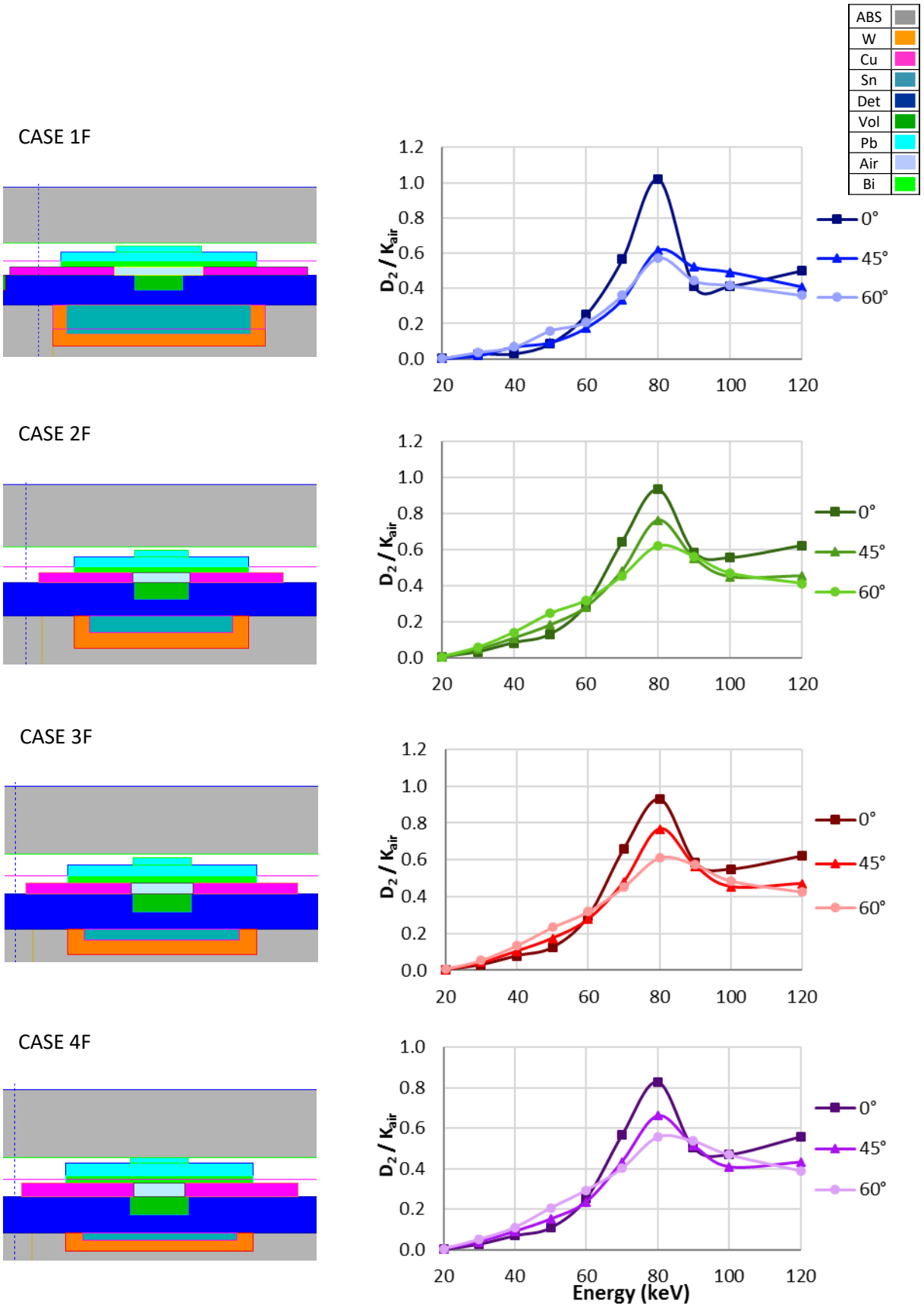

Figure 30. High Z filter configurations and corresponding response of the detecting volume 2 of the realistic dosimeter B in terms of dose per air kerma.

The analisys of the various configurations will be performed by the compoarison of seven dosimeters through the ratio between the combined dose of each dosimeter and the reference values of the effective dose with lead gamrnets.
Table 13 shows the dosimeters with their combinations of the low and high filtration described in the previous paragraphs.

Table 13. List of the seven dosimeters analysed. The dosimeter corresponding to low Z filtration always changes while the one with high Z filtration remains the same for dosimeters from 2 to 5.

Dosimeter configuration	Low-Z filter (Detector 1)	High-Z filter (Detector 2)
DOSIMETER 1	1E	1F
DOSIMETER 2	2E	2F
DOSIMETER 3	3E	2F
DOSIMETER 4	4E	2F
DOSIMETER 5	5E	2F
DOSIMETER 6	6E	3F
DOSIMETER 7	7E	4F

As a starting point of the realistic dosimeter B, the best result of the realistic dosimeter A has been tested in order to see the effects of the reduction of the detecting volumes on the combined dose. The main difference can be seen in the thicknesses of the back filters, which are now less effective also due to the fact that the new detecting volumes don't cover all the height of the detector.

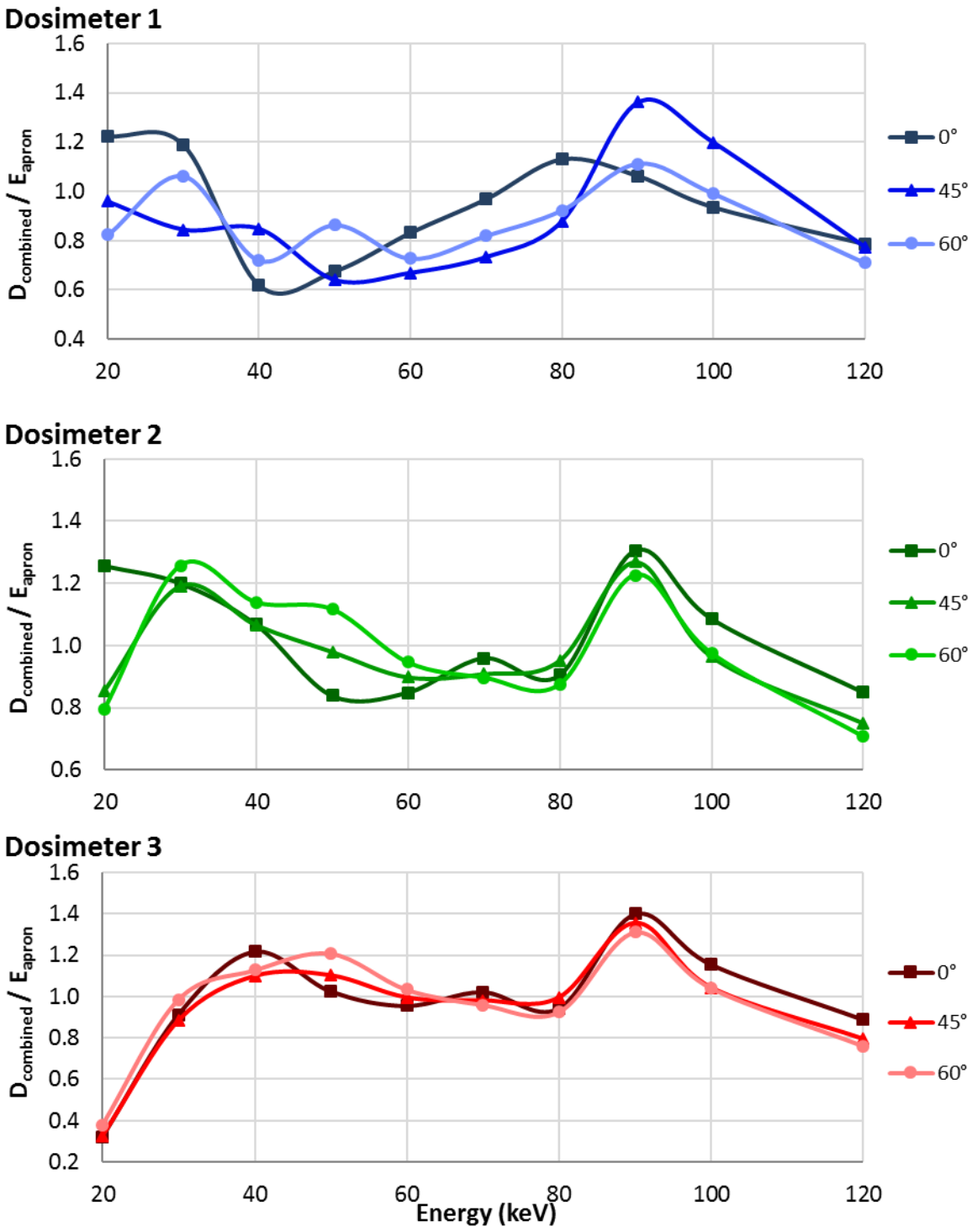

Figure 31. Ratio between the combined dose and the effective dose with lead garments for the seven dosimeters.

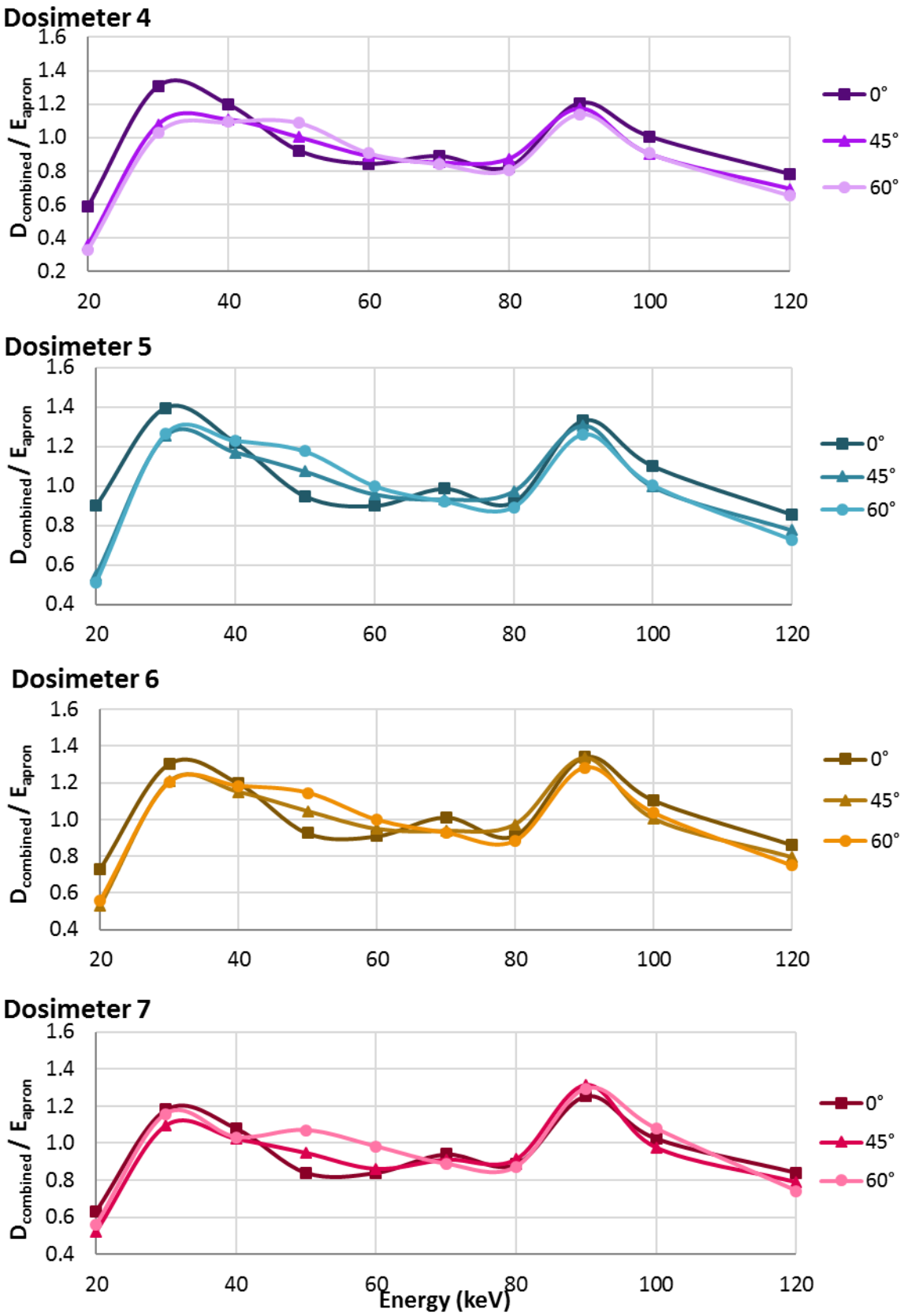

Figure 31 (continuation). Ratio between the combined dose and the effective dose with lead garments for the seven dosimeters.

As already introduced the assumption of the ineffectiveness of the back filters can be justified by the underestimation in the range between 40 and 70 keV. Furthermore, the bigger volume occupied by air above the detector might be the explanation of the peak of overestimation of the curve of $45°$. The constants in case of the dosimeter 1 are α=1/2 and β=1/150.

The result shown in *Figure 31* (dosimeter 2), highlights a great improvement in terms of overestimations and underestimations, which have been reduced up to ±30%. The main modifications have been the reduction of the air above the detecting volume and also the reduction in the *x* direction of the small layer of lead on top. The constants in the case of dosimeter 2 are α=1/2.3 and β=1/120. One of the problems of this configuration is that the constant related to the dose with low Z filtration (β) is still too small.

Dosimeter 3 is similar to the previous one except for the material of the low Z filter, which pass from aluminium to titanium. Titanium has an atomic number higher with respect to aluminium and it has been chosen because the objective is to increase the β constant and thus increase the contribution of the low Z to the combined dose.

With a truncated pyramid made only by titanium, the β constant is considerably increased bringing the ratio between the combined dose and the reference effective dose very close to one from 30 to 80 keV. But a new strong underestimation arises at 20 keV and cannot be fixed only through the modification of the constant. The constants in the case of dosimeter 3 are α=1/2.4 and β=1/40.

From the results of dosimeter 3, a new configuration has been proposed trying to combine the effects of aluminium and titanium. The first attempt has been to introduce two layers, one over the other, taking advantage of both materials.

The high Z configuration is still equal to dosimeters 2 and 3, to simplify the comparison and make the effects of the result evident. This structure is still not satisfying the requirement of reducing the underestimation at low energy but there is an enhancement concerning the peak at 90 keV. The low energy region has still to be improved and the continuous strong underestimation at 20 keV is again due to the too thick layer of titanium; the higher Z doesn't allow many low energy photons to reach the detector. The constants in the case of dosimeter 4 are α=1/2.6 and β=1/50.

The next step is to reduce the dimension of titanium and to insert it in another filter made by aluminium. At the beginning the shape of the truncated pyramid has been chosen also for the titanium filter while the high Z configuration remains the same. The result brought significant improvements in the low energy region and, in addition, the β constant has been increased. The constants in the case of dosimeter 5 are α=1/2.3 and β=1/70.

Dosimeter 6 is characterized by a simplified geometry of the titanium filter, a parallelepiped with respect to the truncated pyramid. In the conditions of a low Z material and for such small dimensions the simplification leads to acceptable results with a gain in terms of manufacturing procedures because of a simpler design. The constants in the case of dosimeter 6 are α=1/2.3 and β=1/70.

In the high Z design of the high Z materials configuration, the thickness and the area of copper have been increased to get over the overestimation at 30 keV. The overall result has only two critic points: the first at 20 keV, which has already been improved, and the peak at 90 keV, which is now a little bit higher because of the increase of the thickness of copper below the three high Z filters made by lead and bismuth.
Anyway, this is a good compromise also considering the behaviour of the curves which is the same for the three angles analysed. This result means that the angular dependence has been very well optimized. The constants in the case of dosimeter 7 are α=1/2.1 and β=1/100.

The last step of the analysis concerning the realistic dosimeter B has been the evaluation of the effective dose using X-ray radiation qualities (*Figure 32*).

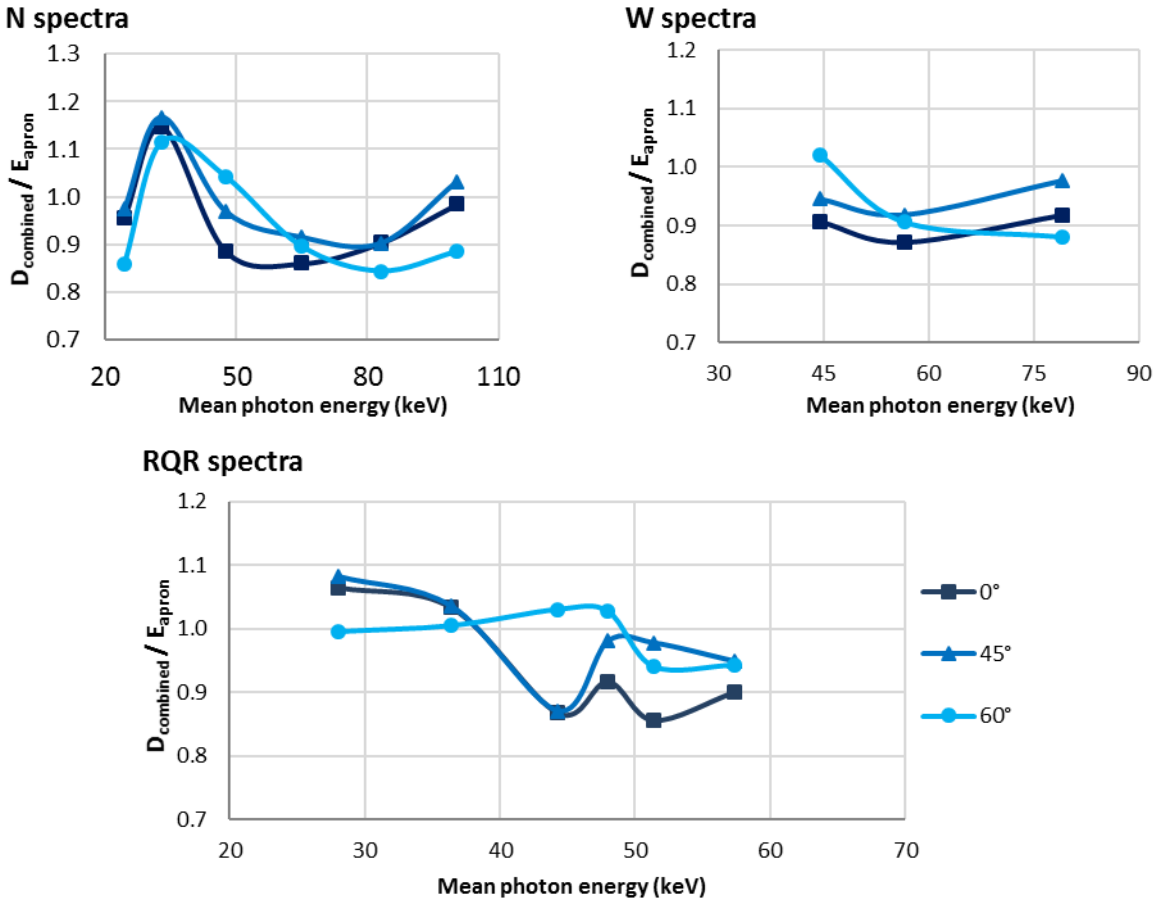

Figure 32. Ratio between the combined dose and the effective dose with RP garments using spectra to reproduce more realistic photon beams in the case of the realistic dosimeter B: N spectra (N30, N40, N60, N80, N100, N120; shown at the top left), W (W60, W80, W110; shown at the top right) and RQR (RQR2, RQR4, RQR6, RQR7, RQR8, RQR9; shown at the bottom).

Figure 32 shows that narrow and wide spectra present very good results with an overestimation and a underestimation in the range of ±15%. Apart from a peak at ~30 keV in the N spectra, fluctuations are minimized. Also RQR spectra presents a very good result,

with a maximum overestimation lower than 10% and a maximum underestimation lower than 15%.

The best realistic configuration is reported in *Figure 33*. This is the dosimeter 7 of the realistic configuration B and it is made by combination of the low Z filtration 7E and the high Z filtration 4F, described in the previous section.

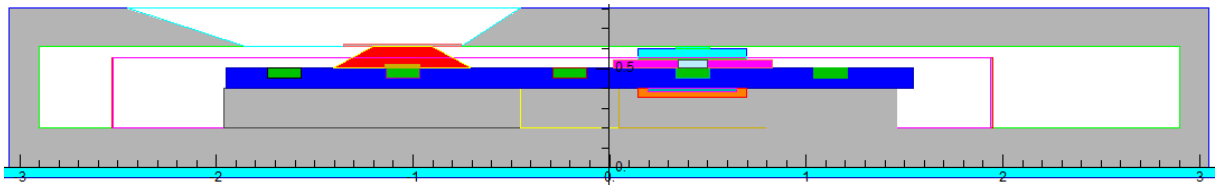

Figure 33. Best design of the realistic dosimeter.

4. CONCLUSION

The results of this study demonstrate that it is possible to design a new whole-body dosimeter able to provide an acceptable estimation of the effective dose with lead garments. This study focused on optimizing the filtration of a whole-body dosimeter based on RPL detectors. The effective dose estimated by the dosimeter is obtained from the dose received by two detector volumes with different filtration.

It has been demonstrated that the dose estimated with a newly designed dosimeter (called dosimeter 7 in case of the realistic dosimeter B) shows a very good agreement with the values of the effective dose with lead garments taken as reference. In particular, the most relevant results are given for photon beams with RQR energy spectra, which are the standard X-ray radiation qualities that represent the best the exposure of medical staff in interventional radiology and cardiology. The estimation of the effective dose compared to the reference values leads to very good level of accuracy, with an overall overestimation lower than 10% and an underestimation below 15%, for photon beams coming from the right direction with mean energy between 20 and 60 keV and for angles of incidence of 0°, 45° and 60° in the transverse plane.

From the simplified dosimeter to the realistic one, many improvements have been introduced. First of all, the amount of material which has to be inserted as filter has been reduced drastically. The shapes of the filters have been simplified because conical or cylindrical geometries have been replaced by parallelepipeds and at most a truncated pyramid. Also, the overall dimension of the dosimeter is the same of the existing one.

The advantage of this new method is the possibility of wearing only one dosimeter over the radioprotective garment, which is more practical, less expensive and reduces the uncertainties related to the use of correction factors or two dosimeters located in different positions (over and below the lead apron).

The thesis concerned the evolution of the design of the new dosimeter from initial feasibility, performed with the first analysis using a simplified dosimeter, to a more realistic development. But some work still needs to be done: the main purpose is to represent all the possible exposure conditions of the medical staff, for this reason the simulations considering the photon beams with an angle of incidence in the transverse plane are not enough. Photon beams in the sagittal plane should also be taken into account, with the beam directions from above and below.

The fact that only two among the five detecting volumes present in the detectors are used, tells that at least other three detecting volumes can be sources for future studies, either in the development of new algorithms combining more than two doses or in the use of the free detecting volumes for other purposes.

Following the Monte Carlo simulations, the final step could be the construction of a prototype and the experimental testing of the same to assess its performance and guide future optimizations.

LIST OF FIGURES

LIST OF TABLES

REFERENCES

[1] ICRP - Publication 103, “The 2007 Reccomendations of the International Commission on Radiological Protection,” 2007.

[2] ICRP - Publication 118, “Statement on Tissue Reactions and Early and Late Effects of Radiation in Normal Tissues and Organs - Threshold Doses for Tissues Reactions in a Radiation Protection Context,” 2012.

[3] SCK•CEN, “Personal dosimetry,” [Online]. Available: http://dosimetry.sckcen.be/en/Our_Services/Personal_dosimetry.

[4] Landauer, “Dosimeters,” [Online]. Available: http://landauer.com/Industry/Products/Dosimeters/Dosimeters.aspx.

[5] IRSN , “Dosimétrie individuelle,” [Online]. Available: http://dosimetre.irsn.fr/fr-fr/nos-produits/dosimetrie-individuelle.

[6] IAEA, “Radiation Protection of Patients (RPOP),” [Online]. Available: https://rpop.iaea.org.

[7] EURADOS CONRAD WP7/SG2, “Double Dosimetry with Recommendations”.

[8] H. Järvinen et al., “Comparison of double dosimetry algorithms for estimating the effective dose in occipational dosimetry of interventional radiology staff,” 2008.

[9] G. Kuipers, X. L. Velders, “Effective dose to staff from interventional procedures: estimation of single and double dosimetry,” 2009.

[10] H. Järvinen et al., “Overview of double dosimetry procedures for the determination of the effective dose to the interventional radiology staff,” 2008.

[11] SCK•CEN, “Development of a personal dosimeter suitable for IR and IC medical staff wearing RP lead garments,” 2015.

[12] ICRP - Publication 119, “Compendium of Dose Coefficients based on ICRP Publication 60,” 2012.

[13] NIST, “The Mass Attenuation Coefficient,” [Online]. Available: http://physics.nist.gov/PhysRefData/XrayMassCoef/chap2.html.

[14] NIST, “The Mass Energy-Absorption Coefficient,” [Online]. Available:

http://physics.nist.gov/PhysRefData/XrayMassCoef/chap3.html.

[15] N. Hocine et al., “Personal monitoring glass badge: theoretical dosemeter response calculated with Monte Carlo transport code MCNPX,” 2011.

[16] D. Maki et al., “Development of the new glass badge,” 2015.

[17] International Organization for Standardization, “ISO 4037-1: X and gamma reference radiation for calibrating dosemeters and doserate meter and for determining their response as a function of photon energy - Part 1: Radiation characteristics and production methods.,” 1996.

[18] International Electrotechnical Commission, “IEC 61267: Medical diagnostic X-ray equipment - Radiations for use in the determination of the characteristics,” 2005.

[19] H. Dang, “Particle induced strand breakage in plasmid DNA,” 2010.

[20] J. K. Shultis, R. E. Faw, “An MCNP primer,” Revision 2010.

[21] A. L. Reed, “Medical physics calculations with MCNP: a primer,” Los Alamos National Laboratory, 2007.